Laboratory of Polymer Chemistry
Department of Chemistry
University of Helsinki
Helsinki, Finland

FUNCTIONAL SURFACES AND NANOPARTICLES BASED ON SEMIFLUORINATED COPOLYMERS

Lauri Valtola

ACADEMIC DISSERTATION
FOR THE DEGREE OF DOCTOR OF PHILOSOPHY

To be presented, with the permission of the Faculty of Science, University of Helsinki, for public criticism in Auditorium A110 of the Department of Chemistry, on 21st November 2014, at 12 o'clock noon.

Helsinki 2014

Opponent

Professor Michael Malkoch
Department of Fibre and Polymer Technology
School of Chemical Science and Engineering
Royal Institute of Technology
Sweden

Reviewers

Professor Matti Elomaa
Centre for Materials Research
Tallinn University of Technology
Estonia

&

Professor Robin Ras
Department of Applied Physics
Aalto University
Finland

ISBN 978-951-51-0275-1 (Paperback)
ISBN 978-951-51-0276-8 (PDF)

Unigrafia
Helsinki 2014

Kun ihminen nukkuu, sille ei tapahdu mitään.
Mutta kun se ei nuku, se voi saada vaikka kalan.
-Matti Nykänen

ABSTRACT

The main objectives of this study were to synthesize semifluorinated polymers and to study their solution and surface properties.

Semifluorinated copolymers were synthesized either by free radical solution polymerization or by using atom transfer radical polymerization, ATRP. Free radical solution polymerizations of eicosanol methacrylate, (EIMA), and perfluorooctyl methacrylate, (FMA) resulted in semifluorinated copolymers with various fluorine contents. Copolymerization reactivity ratios of the monomers were estimated by using Fineman-Ross (F-R) and Kelen-Tüdős (K-T) methods. It was found that the polymers had a random comonomer distribution with some tendency to alternate.

Further, ATRP reactions were used to build up diblock copolymers. First EIMA or styrene, (S), were polymerized and used as macroinitiators to polymerize different fluorine containing monomers, FMA, 2,3,5,6-tetrafluoro-4-(3,3,4,4,5,5,6,6,7,7,8,8,9,9,10,10,10-heptadecafluorodecaoxy)styrene, (FSF), perfluorooctyl-ethylene oxymethyl styrene, (EMS), pentafluorostyrene, (FS).

Both block and random copolymers bearing CF_3 showed high surface activity in toluene and had critical micellization concentration (CMC) below 0.5 wt%. Above the CMC aggregates with sizes ranging from 10 nm to 100 nm were observed by dynamic, (DLS), and static light scattering, (SLS). Combined LS and TEM studies showed that due to the rigidity of fluorinated blocks the aggregates were ellipsoidal when dispersed without heating but shrunk to spherical aggregates upon heating.

Fluorinated surfaces and particles of the block copolymers were made by solvent casting, electrospinning or breath figure templating (BF). All produced surfaces were hydrophobic (contact angle of water, CA_{water} >100°). When the surface roughness was increased *e.g.* by electrospinning or breath figure templating, it was possible to turn some surfaces superhydrophobic (CA_{water} >150°) and their lipophobic properties were enhanced. Such films with enhanced hydro- or oleophobic characteristics may find application for example as dirt repelling surfaces or bringing anticorrosive properties to coatings.

One of the studied block copolymers, polystyrene-block-polypentafluorostyrene (PS-*b*-PFS) was modified with glucose or carboxylic acid moieties via thiol click reaction. These polymers were then prepared as porous BF films or made to nanoparticles with varying sizes (diameter 100 to

360 nm) utilising solvent exchange or aerosol technique. The introduction of glucose or carboxylic acid functionalities rendered the porous surfaces made of these polymers hydrophilic while the films with PS-*b*-PFS were hydrophobic. It was shown that the sugar residues in the pores of BF films or on the nanoparticles are capable of binding fluorescent markers, lectin ConA-FITC and rhodamine B isothiocyanate (RITC) either via biorecognition or chemical reactions enabling the use of these materials for example in diagnostics applications.

ACKNOWLEDGEMENTS

This work has been carried out in the Laboratory of Polymer Chemistry, University of Helsinki during the years 2005-2013, under the supervision of Professor Heikki Tenhu and Dr. Sami Hietala. The work was funded by TEKES, Magnus Ehrnrooth Foundation, Fortum Foundation and Finnish Cultural Foundation.

I wish to thank Professor Heikki Tenhu for his guidance during these years. I cannot thank enough Dr. Sami Hietala who has given me so much guidance and attention during this work. I would even go fishing with you.

I thank Professor Robin Ras and Matti Elomaa for the thorough and careful review of my thesis.

I am also very grateful to Dr. Peter Denifl, Professor Carl-Erik Wilen, Dr. Antti Laukkanen, Professor Arto Urtti, M.Sc. Mikko Karesoja, M.Sc. Anu Alhoranta, M.Sc. Melina Malinen, Professor Jouko Peltonen, Dr. Petri Ihalainen, M.Sc. Jawad Sarfraz, Dr. Janne Raula and M.Sc Antti Rahikkala for their collaboration and insights regarding the thesis.

The special thank goes also to Professor Sirkka-Liisa Maunu, Dr. Vladimir Aseyev, Seija Lemettinen, Juha Solasaari, Ennio Zuccaro for guidance in every problem you can imagine.

I have been privileged to work with such a nice environment and you all coworkers are resbonsible of it. Just to mention few names: SP, Miia, Teemu, Jukka, Erno, Tommi, Pirita, Helena, Joonas, Tina, Fabian, Pete, Szymon. I am sorry if I have forgotten someone. I really had a great time with you.

Dr. Jari Kavakka needs to be mentioned separately. He is the one who knows everything about organic chemistry, but he is also great friend.

I also want to thank my family for all the support and help you have been given me for the whole of my life. There has always been place to go no matter what has happened.

Of course I have to thank my squash buddies who have kept my life in balance.

Finally my greatest thanks goes to Maija, Lenni and Leevi, with your love I can do anything.

CONTENTS

LIST OF ORIGINAL PUBLICATIONS

This thesis is based on the following publications:

I Lauri Valtola, Sami Hietala, Heikki Tenhu, Peter Denifl, Carl-Eric Wilen. **Association Behavior and Properties of Copolymers of Perfluorooctylethyl Methacrylate and Eicosanyl Methacrylate** Polymers for Advanced Technologies, 2009, 20, 225-23.

II Lauri Valtola, Anu Koponen, Mikko Karesoja, Sami Hietala, Antti Laukkanen, Heikki Tenhu, Peter Denifl. **Tailored surface properties of semi-fluorinated block copolymers by electrospinning.** Polymer, 50, 2009, 3103-3110.

III Lauri Valtola, Mikko Karesoja, Heikki Tenhu, Petri Ihalainen, Jawad Sarfraz, Jouko Peltonen, Melina Malinen, Arto Urtti, Sami Hietala. **Breath figure templated semifluorinated block copolymers with tunable surface properties and binding capabilities.** Journal of Applied Polymer Science, 132, 2015, 41225.

IV Lauri Valtola, Antti Rahikkala, Janne Raula, Esko Kauppinen Heikki Tenhu, Sami Hietala. **Synthesis and Lectin Recognition of Glycosylated Amphiphilic Nanoparticles.** European Polymer Journal, 59, 2014, 282-289.

The publications are referred to in the text by their roman numerals.

The author's contribution to the papers:

In all papers Valtola participated in planning of the study, synthesized and characterized the polymers and analyzed the results. In papers I and II, the author executed all experiments apart from TEM, SEM and electrospinning. In papers III and IV, the author performed all experiments apart from SEM, TEM, AFM, confocal microscopy and production of nanoparticles via aerosol method.

ABBREVIATIONS AND SYMBOLS

F_a, F_b	Molar fractions of a and b in the copolymer.
f_a, f_b	Initial molar fractions of a and b in the feed
k_{act}	Rate constant of activation
k_{deact}	Rate constant of deactivation
k_p	Rate constant of propagation
k_t	Rate constant of termination
M_a^* and M_b^*	Propagating species
M_n	Number average molecular weight
M_w	Weight average molecular weight
N_{agg}	Aggregation number
r_a, r_b	Reactivity ratios
R_g	Radius of gyration
R_h	Hydrodynamic radius

AFM	Atomic force microscopy
AIBN	Azobisisobutyronitrile
ATRP	Atom transfer radical polymerization
BF	Breath figure
CA	Contact angle
CMC	Critical micelle concentration
ConA-FITC	lectin-fluorescein isothiocyanate conjugate from Canavalia ensiformis
DHFOMA	1H,1H-perfluorooctyl methacrylate
DLS	Dynamic light scattering
DMF	Dimethylformamide
EGMAFO	ethylene glycol mono-methacrylate mono-perfluorooctanoate
EIMA	Eicosanol methacrylate
EMS	Perfluorooctyl-ethylene oxymethyl styrene
FDA	1,1,2,2-tetrahydroperfluorodecyl acrylate
FHMA	1,1-dihydroperfluoroheptyl methacrylate
FNEMA	2-[(perfluorononenyl)oxy]ethyl methacrylate
F-R	Fineman-Ross method
FMA	Perfluorooctyl ethyl methacrylate
FRET	Fluoresence energy transfer
FS	Pentafluorostyrene
FSF	2,3,5,6-tetrafluoro-4-(3,3,4,4,5,5,6,6,7,7,8,8,9,9,10,10,10-heptadecafluorodecaoxy)styrene
FT-IR	Fourier transform infrared spectroscopy
HEMA	Hydroxyethyl methacrylate
K-T	Kelen-Tüdős method
GTP	Group transfer polymerization

MMA	Methyl methacrylate
NaMA	Sodium methacrylate
NFHMA	Nonafluorohexyl methacrylate
NMR	Nuclear magnetic resonance spectroscopy
PDI	Polydispersity index
PFOMA	Poly(1,1,2,2-tetrahydroperfluorooctylethyl methacrylate)
PMAGlc	poly(3-O-methacryloy-α,β-D-glucopyranose
PMDETA	N,N,N′,N′′,N′′-pentamethyldiethylenetriamine
PMMA	Poly(methyl methacrylate)
PEO	Poly(ethyleneoxide)
PS	Polystyrene
PS-b-PFS	Polystyrene block polypentafluorostyrene
RAFT	Reversible addition fragmentation chain transfer polymerization
RITC	Rhodamine B isothiocyanate
SANS	Small-angle neutron scattering
SEC	Size exclusion chromatography
SEM	Scanning electron microscopy
SH-GlcAc4	2,3,4,6-tetra-O-acetyl-1-thio-β-D-glucopyranose
SLS	Static light scattering
S	Styrene
TFEMA	2,2,2-trifluoroethylene methacrylate
THFOMA	1H,1H,2H,2H-perfluorooctyl methacrylate
TEM	Transmission electron microscopy
THF	Tetrahydrofuran
UV-vis	Ultraviolet-visible spectroscopy
XPS	X-ray photoelectron spectroscopy

1 INTRODUCTION

Chemistry of fluorous compounds started to develop in 1930's when the first drops of a liquid perfluoroalkane were produced in synthesis. The unique properties of fluorinated compounds, such as their high density and high surface activity were soon discovered.[1] The term perfluorinated indicates that all hydrogen atoms are replaced by fluorine atoms in the molecule while in semifluorinated compounds there are still hydrogen atoms present.

Polymers composed of flexible backbones having semi- or even perfluorinated alkyl side chains have unique and interesting characteristics, which originate from the nature of the C-F bonds as well as the fluorine atoms.[2-5] Fluoroalkyl groups are generally insoluble in water and most organic solvents. One possible way to increase the solubility of these materials is copolymerization of fluorine containing monomers together with nonfluorinated ones. This approach has resulted in a number of different copolymers, where fluorinated chain ends or random or block distribution of the fluorinated monomers in the polymer chains gives rise to new properties, such as amphiphilicity and tendency for microphase separation. The development of living/controlled polymerization techniques has allowed straightforward synthesis of various block copolymers with fluorinated segments. Especially atom transfer radical polymerization (ATRP) has been successfully used to synthesize various fluorinated (meth)acrylic and styrenic block copolymers with low dispersities and tailored molecular architectures including star-like or hyperbranched topologies.[3] On the other hand, a class of fluorinated polymers contain aromatic fluorinated rings, such as pentafluorobenzene (FS),[6] instead of a fluorinated alkyl chain. These polymers share the common properties brought by the C-F bonds and fluorine atoms. However, as FS does not contain the most surface active CF_3 groups, polymers based on for example pentafluorostyrene tend to be more soluble in organic solvents. The aromatic groups may also be functionalized with fluorinated alkyls, resulting in highly fluorinated monomers.[7-9] Similarly as the fluoroalkyl polymers, the block copolymers based on fluorinated polystyrenes tend to microphase separate due to the incompatibility of the blocks.

In general, semifluorinated polymers may have amphiphilic nature and can be used as surfactants. The term amphiphilic implies attraction to two different kinds of media. The surfactant structure can be described as consisting of two parts with vastly different solution characteristics: "a solvent-soluble" lyophilic part and "a solvent-insoluble" lyophobic part. Conventional surfactants consist of a water-soluble hydrophilic part and a

water-insoluble hydrophobic part, which is lipophilic, compatible with fats and hydrocarbons.

In semifluorinated polymers the lyophobic part of the molecule contains fluorine and the hydrocarbon part is lyophilic. Fluorinated surfactants having water soluble parts can decrease the surface tension of water below the lower limit reached by purely hydrocarbon-type surfactants. In addition the fluorinated hydrophobes are more resistant to chemical attack. Therefore fluorinated surfactants are commonly used in media where conventional surfactants are not applicable. Partially fluorinated non-ionic hydrocarbons may be used as surfactants in non-aqueous media due to their amphiphilic nature. In concentration regimes where aggregates (micelles, reverse micelles or vesicles) are formed, a phase separated dispersion is obtained. The absence of water in these systems gives an advantage as reaction media for moisture sensitive reactions. The application of semifluorinated surfactants in the emulsification of reaction mixtures for example in liquid or supercritical carbon dioxide[10] or other organic or fluorinated solvents,[11-13] and stabilisation of oil-in-oil[14] emulsions has been reported. The properties of these macromolecules make them possible substances to be used as gelling or foaming agents for various organic solvents.[15-19] Semifluorinated materials exhibit many desirable physical properties, such as high surface activity, enhanced chemical resistance and high thermal stability[5] and can be used in a variety of applications, e.g. as low dielectric constant polymers in electronic industry,[20] polymeric optical waveguides,[21,22] friction modifiers in lubrication oil,[23] surface modifiers[24] and in membranes.[25]

Although fluorinated compounds are often chemically inert, the aromatic pentafluorostyrene can be used for variety of reactions. One of such reactions, called thiol-para fluorine click reaction, is interesting due to its efficiency under mild reaction conditions.[26-30] It is especially convenient as a post-modification reaction, as the synthesis of well-defined poly(pentafluorostyrene) copolymers is easily accomplished with many schemes[6,31-38] and the reaction can be easily monitored e.g. via ^{19}F NMR.[26,39] Also, a large number of thiol reagents that can be used in the functionalization of pentafluorostyrene units are commercially available. Utilizing thiol-para fluorine click chemistry it is possible to produce for example glycopolymers bearing sugar functionalities with well-defined structures to be used in different kinds of applications such as sensing or separation materials.

1.1 SYNTHESIS OF SEMIFLUORINATED POLYMERS

A variety of semifluorinated polymer structures are found in the literature, from homopolymers to block, random, graft and starlike polymers. Semifluorinated polymers can be prepared with copolymerization of fluorinated and non-fluorinated monomers for example via conventional free radical polymerization,[40-45] atom transfer radical polymerization (ATRP),[6,37,46-60] reversible addition–fragmentation chain-transfer polymerization (RAFT),[61-63] nitroxide mediated polymerization (NMP),[8,9,64,65] living cationic,[66-72] living anionic[3,73,74] and group transfer polymerization (GTP).[75] Various styrenic[6,37,59,76-79] as well as acrylate[8,48,61] and methacrylate[46,47,49,50,53,55,62,74,80] based fluorinated monomers can be polymerized via these mentioned methods.[40-43,81-85] While controlled polymerization techniques may lead to block copolymers, for traditional free radical copolymerizations it has been found that in most cases random polymers with somewhat alternating structures are obtained.[40-43] Scheme 1 presents chemical structures of two commonly used fluorinated monomers pentafluorostyrene and 3,3,4,4,5,5,6,6,7,7,8,8,9,9,10,10,10-heptadecafluorodecyl acrylate.

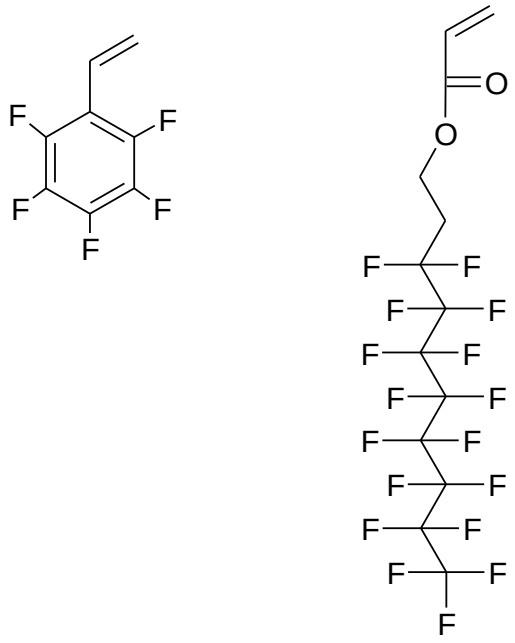

Scheme 1. Chemical structure of pentafluorostyrene and 3,3,4,4,5,5,6,6,7,7,8,8,9,9,10,10,10-heptadecafluorodecyl acrylate.

1.1.1 REACTIVITY RATIOS IN FREE RADICAL COPOLYMERIZATION

Copolymer properties depend largely on their structure, *i.e.* the molar ratios of the repeating units and their sequence distribution. Different monomers may have different reactivities in the polymerization process, sometimes ruling out copolymerization of certain monomers, leading to alternating or random structures or even block copolymers. Therefore the structure of the produced copolymer may differ drastically from the monomer feed of polymerization. In order to estimate the structure of copolymers the determination of the reactivity ratios of monomers (r_a and r_b) is a viable method. Since, copolymers consists of at least two different repeating units, they can be classified according how these repeating units are arranged in polymer chain. The parameters r_a and r_b are defined as the ratio of the rate constant for the propagating species when adding the own type monomer to the rate of the adding other type monomer. In ideal copolymerization $r_a r_b = 1$. This means that two types of propagating species M_a^* and M_b^* show equal tendency for adding monomer 1 or monomer 2.

In alternating copolymerization $r_a = r_b = 0$ two monomers polymerize in equimolar amounts with alternating arrangement.

If the reactivity ratios of two monomers are $r_a > 1$ and $r_b > 1$, there is tendency to form block copolymers.

Reactivity ratios are determined by following the reaction rates of monomer species. This can be done for example by the use of high resonance ^{1}H NMR technique.[81,86] Usually data from low conversions are used to minimize the errors. Other methods to characterize reactivity ratios include elemental analysis[87] and other spectroscopy methods like UV-vis[88] or IR.[89]

One way to do the reactivity ratio analysis is to use methods developed by Fineman and Ross (F-R)[90] and Kelen and Tüdős et al. (K-T).[91]

The Fineman-Ross equation (F-R) gives an estimation of the reactivity ratios r_a and r_b according to

$$G = r_a H - r_b \qquad (1)$$

Where $G=x(X-1)$ and $H=x^2/X$. $x=f_a/f_b$ where f_a, f_b are the initial molar fractions of A and B in the feed. $X=F_a/F_b$ where F_a, F_b are molar fractions of A and B in the copolymer. Each copolymerization gives one point (G,H) and a straight line is expected to pass through these points. The slope of this line gives r_a and the ordinate intercept is r_b.

The Kelen- Tüdős equation (K-T):

$$\eta = (r_a + \alpha)\xi - r_b/\alpha \qquad (2)$$

Where, $\eta = G/(\alpha + H)$, $\xi = H/(\alpha + H)$, $\alpha = (H_{max} * H_{min})$. The slope of this line gives $r_a + \alpha$ and the ordinate intercept gives $-r_b/\alpha$. Successful determination of monomer reactivity ratios gives tools for the estimation of molecular composition of formed copolymer.

1.1.2 ATOM TRANSFER RADICAL POLYMERIZATION OF FLUORINATED MONOMERS

ATRP is a controlled radical polymerization method. It was reported separately in 1995 by Sawamoto's group[92] and by Wang and Matyjaszewski.[93] The most important step in ATRP mechanism is the reversible cleavage of the carbon-halide bond in the dormant species via a redox process. This process is catalysed by a transition metal complex, see Scheme 2.

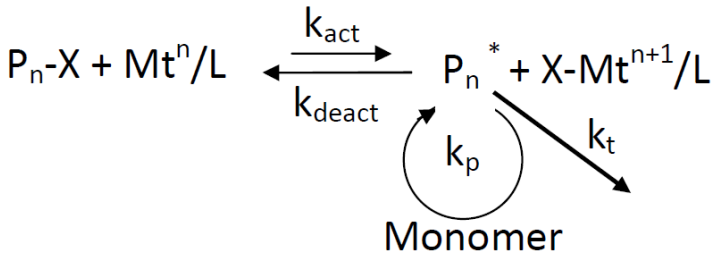

Scheme 2. Mechanism of ATRP.[93]

The transition metals that usually are used are ruthenium, iron or copper. Initiation system in ATRP consists of transition metal/ligand complex and initiator. Initiators typically are alkyl halides as shown in Scheme 3.

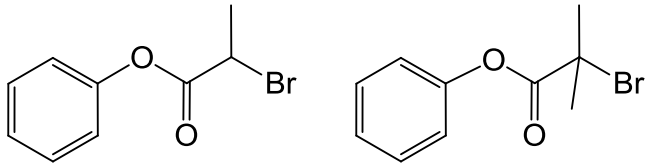

Scheme 3. Typical ATRP initiators.

ATRP is one of the most used controlled polymerization techniques. The reason for its popularity is the experimental simplicity and the availability of initiators and catalysts. DeSimone and co-workers reported several examples of the polymerization of 1H,1H-perfluorooctyl methacrylate (FOMA) by ATRP using different kinds of macroinitators made also by ATRP.[46] ATRP of fluorinated monomers has also been used in supercritical CO_2,[47] a solvent in which fluorinated monomers and polymers are soluble. Haddleton and his

group have studied ATRP of 2,2,2-trifluoroethylene methacrylate (TFEMA) and perfluorooctylethyl methacrylate (FMA). These homopolymers were also used as macroinitiators for methacrylates.[49,50] Poly(1,1,2,2-tetrahydroperfluorooctyl methacrylate) (PFOMA) was prepared by Yang *et al.* with ATRP.[51] Shemper *et al.* used ATRP to polymerize perfluorooctylethyl methacrylate (FMA) homopolymers and copolymers together with poly(propylene glycol) methacrylate.[52] Lim *et al.* used PEO macroinitiators to polymerize 1H,1H-perfluorooctyl methacrylate (DHFOMA), and 1H,1H,2H,2H-perfluorooctyl methacrylate (THFOMA) to be used as surfactants in supercritical carbon dioxide-water emulsions.[53] Hussain *et al.* prepared di- and triblock copolymers via ATRP by using PEO macroinitiators and perfluorohexylethyl methacrylate as fluorinated monomer.[54,55] Zhang *et al.* prepared di- and triblock copolymers via ATRP using 2-[(perfluorononenyl)oxy]ethyl methacrylate (FNEMA) and ethylene glycol mono-methacrylate mono-perfluorooctanoate (EGMAFO) as fluorinated monomers.[56,57] These block copolymers showed great potential to be used as surfactants, water- and oil-repellent agents.

Radhakrishnan *et al.* synthesized surfactants for supercritical CO_2 applications and they used different kinds of styrene based monomers, which were further polymerized via ATRP.[58] Jankova and Hvilsted polymerized styrene and pentafluorostyrene di-, tri-, and pentablock copolymers via ATRP.[37,59] Hvilsted *et al.* also synthesized pentafluorostyrene based monomer by adding fluorinated alkyl chain in the para position of pentafluorostyrene. Monomer was further polymerized via ATRP to produce materials with low surface energy.[6] Fu *et al.* used ATRP to polymerize pentafluorostyrene homopolymers and diblockcopolymer with *tert*-butyl acrylate.[60] *Tert*-butyl acrylate was further hydrolyzed to polyacrylic acid to yield amphiphilic block copolymer. Ma and Lacroix-Desmazes synthesized block copolymer consisting PEO block and 1,1,2,2-tetrahydroperfluorodecyl acrylate (FDA) block to be used as surfactants in supercritical and liquid CO_2-water emulsions.[61]

1.2 SOLUTION PROPERTIES OF FLUORINATED POLYMERS

Usually fluorinated homopolymers are poorly soluble in common organic solvents. Solubility can, however, be increased by copolymerization of fluorinated monomers together with an organo-soluble monomer. The fluorinated macromolecules have some advantageous properties. In particular, they possess higher surface activity compared with ordinary non-fluorinated polymers at water-air, water-oil or oil-air interfaces. The

investigation of these systems is therefore important for the study and development of oil-in-oil dispersions for example as medium for catalysis.

Surface tension of organic solvents is generally decreased by semifluorinated copolymers. The efficiency of the surface tension reduction is generally increased by the length of the fluoroalkyl chain.[94] Morita et al.[11] studied the effect of varying concentrations of the fluorinated surfactants on interfacial surface tension of toluene and perfluoropolyether emulsions and found out that there was no direct correlation between the depression of surface tension and emulsion stabilities. Various molecular assemblies, such as monolayers, bilayers, regular and reversed micelles or vesicles can be formed due to self-organization of semifluorinated block copolymers in organic, aqueous and fluorocarbon or even in solvent mixtures. [14,15,37,45,53,54,80,82,85,95-104] Light scattering studies have shown that low molar mass semifluorinated block copolymers form micelles/aggregates of size of a few nm in perfluorooctane,[96] perfluortributylamine,[95] perfluorooctane/isooctane mixtures[18] and dodecane.[15] When the chain length is increased, semifluorinated block copolymers form larger aggregates or micelles in the size range of tens to hundreds in nm addition to unimers in chloroform,[53,80,97] acetonitrile,[97] or supercritical CO_2.[98] Side chain fluorinated alkyl chains may pack with each other which increases the stiffness of the polymer backbone and may lead to non-spherical structures.[53,80,99] For random copolymers well defined aggregation of micelles is usually not expected. However, due to the fact that fluorinated units are strongly incompatible with the hydrocarbon parts and the solvent, the polymers tend to aggregate.

1.3 FLUORINATED SURFACES

Fluorocarbon materials possess low surface energy. This property combined with possible surface structuring makes it possible to achieve very oleophobic or hydrophobic surfaces. One application that has raised interest for fluorocarbon materials are thus hydrophobic surface coatings.[105,106] Partially due to the specific properties of fluorocarbon materials these surfaces display repelling properties and could be utilised as coatings with anti-fouling or self-cleaning activity.[107] Fluorinated surfaces have also application in medicine, in systems where protein repellency is needed. Jie Gao *et al.* studied fluorinated films, for which fluorinated FMA end-capped poly n-alkyl methacrylate polymers were synthesized via ATRP method.[108] Van de Grampel *et al.*[83] studied surface energy of coatings by copolymerization of commonly used monomers such as methyl methacrylate with fluorine-containing monomers. The surface energy (mNm^{-1}) of copolymers of 1,1-dihydroperfluoroheptyl methacrylate (FHMA) and methyl methacrylate

(MMA) decreases sharply with increasing FHMA content, resulting in a reduction of the surface energy by a factor about 2 at an incorporation of 15 mol% of FHMA. Same trends were observed for copolymers using styrene and fluoroalkyl-modified styrene.[109]

1.3.1 SURFACE WETTING

Lipophobic and hydrophobic surfaces have found application in a variety of settings, including self-cleaning surfaces, prevention of snow sticking, oxidation and heat conduction processes, among others.[110-112] Superhydrophobic surfaces are defined as having contact angle of water above 150°. In nature superhydrophobic behavior is found for example in plant leaves,[113] thus often described as the lotus leaf effect, where the topography of the surface together with chemical properties gives rise to the property. Lotus leaf effect can thus be achieved without non-fluorinated materials, but requires careful optimization of the structures. With fluorinated compounds superhydrophobicity is achievable without as stringent structure optimization due to their inherent hydrophobicity.[114] Though fluorinated compounds are good candidates for components for superhydrophobic surfaces, surface roughness is usually required as well to achieve superhydrophobicity.

1.3.2 ELECTROSPINNING

Electrospinning or electrospraying is a process by which either submicron polymer fibers or polymeric particles can be deposited on a surface using electrostatically driven jet of a polymer solution.[104-106,115-118] If the molecular weight of the polymer is high enough and viscosity of the solution appropriate, mats of solid polymer (nano)fibers on the surface of choice can be achieved. If the polymer chains are too short to make chain entanglements during the process, typically micronsized particles are formed instead of fibers. These surfaces typically have the roughness needed to observe superhydrophobicity. Ma *et al.*[105] coated electrospunned polycaprolactone with poly(perfluoroalkyl ethyl methacrylate) by initiated chemical vapor deposition to yield super hydrophobic fibers with contact angle of water 175°. Agarval *et al.*[106] compared surfaces made by spincoating and electrospinning of polypentafluorostyrene. A change from spincoating to electrospinning yielded a shift from hydrophobic to superhydrophobic surfaces. Guo *et al.*[115] fabricated superhydrophobic films by electrospraying poly(methyl methacrylate)-*b*-poly(dodecafluoroheptyl methacrylate) diblock copolymers. Grignard *et al.*[118] prepared superhydrophobic aluminum surfaces with excellent corrosion resistance by electrospinning of block copolymer consisting of poly(heptadecafluorodecyl acrylate-*co*-acrylic acid) random

copolymer as the first block and poly(acrylonitrile) as the second one. Carboxylic moieties anchor the polymer to the aluminum surfaces after heat treatment, while fluorinated moieties promote hydrophobicity. Poly(acrylonitrile) block was selected to ensure the stability of surface structure during heat treatment.

1.3.3 BREATH FIGURE FILMS

Highly structured, porous polymeric films made via "breath figure technique" have gained considerable interest[119-121] since the reports by Francois and coworkers.[122,123] In breath figure technique a solution of polymer is typically deposited on a substrate in a humid atmosphere so that the evaporation of the volatile solvent causes the decrease in temperature in the polymer solution. Water droplets start to condensate at the air/liquid interface. As the solvent continues to evaporate, the droplets grow and self-organize into an array. If proper conditions are achieved the water droplets do not coalesce because the concentrated polymer solution keeps them separated. When the solvent evaporates completely, the polymer forms a mold around the water droplets. This is followed by the total evaporation of water molecules and an array of pores in the polymer film is formed.

The breath figure formation has been shown to work in many different systems. Casting conditions, solvents, surfaces and polymers can be varied.[119-121,124-126] The first reports of polymer films prepared by the method were based on star-like polystyrene[122] and it has been stated that polymers that adopt a spherical shape are beneficial for the generation of regular porous structures.[120,121] Also the balance between hydrophilic and hydrophobic properties of the polymers can be used to alter the obtained morphology.[120,121] Although even homopolymers have been shown to produce porous films through BF technique, aggregated amphiphilic block copolymers in a selective solvent are a natural choice for such templating method. The breath figure formation of various amphiphilic diblock copolymers comprising a hydrophobic and a hydrophilic block[127-132] have been studied using various solvents for the templating. Recently the breath figure formation of mixtures of different polymers, namely a mixture polystyrene-*block*-polypentafluorostyrene, polystyrene-*block*-poly[poly(ethylene glycol) methyl ether methacrylate] and high molar mass polystyrene as the matrix[133] has been reported. The combination of these polymers resulted in pores with varying hydrophilicity due to phase segregation of the blocks.

Porous block copolymer films can be used in several applications. The pores and their regular arrangement can be utilized to obtain for example photoluminescence, biorecognition or cell adhesion as well as

superhydrophobicity.[121] For applications it would be beneficial to tailor the hydrophilicity or the hydrophobicity depending on the desired application. It can be done in the case of amphiphilic polymers by selecting the right templating parameters and for example selectively promote or prevent cell or biomolecule adhesion.[134-136] The surface properties of honeycomb structures have been modified by changing the casting conditions for a poly(pentafluorostyrene)-*b*-polystyrene-*b*-poly[poly(ethylene glycol) methyl ether methacrylate] triblock copolymer[137,138] so that either hydrophobic or hydrophilic segments are oriented towards the surface. Further, the honeycomb structures can also be modified by stripping the outer layer of the polymer film made from poly(methyl methacrylate-*co*-perfluoro octyl ethyl methacrylate)[139] or polystyrene-*b*-poly(2-vinylpyridine)[140] with an adhesive tape. The resulting needle-like surface lead to superhydrophobicity and also enhanced lipophobic properties of the film due to the increased surface roughness.

2 OBJECTIVES OF THE STUDY

The main objectives of the present research were the synthesis and characterization of organosoluble semifluorinated copolymers from various monomers. Polymers were synthesized either by free radical solution polymerization yielding random copolymers or by atom transfer radical polymerization to build up block structures.

The polymers were characterized carefully and their ability to act as surfactants was studied. Secondly, electrospinning and breath figure techniques were used to make structured coatings aiming at superhydrophobicity and oleophobicity. These structured films were compared with flat films made by solvent casting. Breath figure films were further modified with hydrophilic moieties. Surfaces were all carefully characterized and their wetting properties were studied. This kind of manipulation of surface may lead to applications in biorecognizing surfaces, cell culturing, superhydrophobic surfaces and lithography. Biorecognition was studied with two sugar binding fluorescent markers, lectin ConA-FITC and rhodamine B isothiocyanate (RITC). ConA has an ability to bind sugars via specific protein-sugar interactions and rhodamine B via chemical reactions.

Finally, glucose-decorated nanoparticles were prepared via nanoprecipitation and aerosol preparation. The effect of nanoparticle size and their surface glucose content on the lectin recognition efficiency was investigated.

3 EXPERIMENTAL

This section summarizes the synthetic methods and the characterization of all monomers, homopolymers and copolymers used during the work. Also the post-functionalization of the polymers is described. The methods to prepare electrospun surfaces and nanoparticles prepared by solvent exchange or aerosol technique, as well as films with breath figure technique are discussed.

3.1 MONOMER SYNTHESIS (I, II)

Styrene (S), pentafluorostyrene (FS) and perfluorooctyl ethyl methacrylate (FMA) were commercially available and were distilled in reduced pressure to get rid of inhibitors and impurities. Eicosanol methacrylate (EIMA) was prepared by the reaction of 1-eicosanol and methacryloyl chloride with 71 % yield. Synthesis of 2,3,5,6-tetrafluoro-4-(3,3,4,4,5,5,6,6,7,7,8,8,9,9,10, 10,10-heptadecafluorodecaoxy)styrene (FSF) were synthesized by the reaction of 1H,1H,2H,2H-perfluorodecanol and pentafluorostyrene with 30 % yield. Synthesis of perfluorooctyl-ethylene oxymethyl styrene (EMS) was prepared by following the procedure described by Höpken and Möller[109] with 50 % yield.

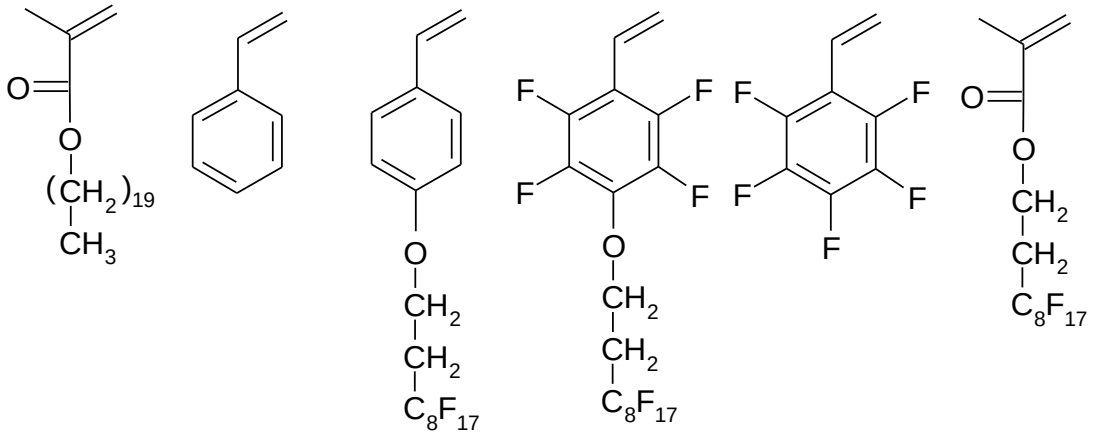

Scheme 4. Monomers used in this work.

3.2 POLYMER SYNTHESIS

3.2.1 FREE RADICAL POLYMERIZATION (I)

Free radical polymerizations were done in toluene by using AIBN as a initiator. Polymerization conditions and characteristics are listed in table 1.

Table 1. Characteristics and polymerization conditions of free radical polymerizations.

Polymer	FMA (g)	EIMA (g)	AIBN (mol%)	V (ml)	T (^oC)	t (hr)	Yield (%)	M_n ($gmol^{-1}$)	PDI	FMA[a] (wt%)
P(EIMA)	0	5	0,7	36	50	168	96	54000	2,7	0
P(EIMA-FMA)-10%	0,25	2,75	3,4	18	70	24	92	14200	2,9	11,3
P(EIMA-FMA)-20%	0,3	1,5	3,4	10,8	70	24	91	14600	2,4	22,1
P(EIMA-FMA)-30%	1	2	3,4	18	70	24	90	16700	2,1	30,2
P(EIMA-FMA)-50%	1,5	1,5	3,4	18	70	24	71	16800	2	51,2
P(EIMA-FMA)-60%	5	3	3,4	48	70	24	74	6700	1,6	62,3

M_n and PDI is determined by SEC with THF and calibrated againts PMMA standards. [a]Determined by 1H NMR in chloroform

3.2.2 ATRP MACROINITIATORS (I, II, III)

ATRP was used to synthesize bromine terminated macroinitiators. P(EIMA)-Br was synthesized in xylene by using phenyl 2-bromo isobutyrate as initiator and 2,2-bipyridine as ligand. Monomer/initiator /Cu(I)Br/ligand molar ratio was selected to be 50:1:1:2. SEC was used to measure the M_n and PDI using PMMA standards. Bromine terminated polystyrenes were prepared in bulk by using phenyl 2-bromopropionate as initiator and PMDETA as ligand. Monomer/initiator /Cu(I)Br/ligand molar ratio was selected to be 100:1:1:2. SEC was used to measure M_n and PDI of the PS-Br polymers using PS standards.

3.2.3 ATRP COPOLYMERIZATION (I, II, III)

The macroinitiators were chain extended using different monomers. Table 2 collects the polymerization conditions and Table 3 collects the molecular characteristics of block copolymers.

Table 2. Polymerization data of block copolymers.

Polymer	Publication	M (mmol)	Initiator (mmol)	CuBr (mmol)	Ligand (mmol)	Solvent (ml)	Time (min)	Yield (%)
PEIMA-*b*-PFMA	I	2,5	0,05	0,05	0,25[c]	5[a]	90	67
PS28-*b*-PFSF4	II	0,9	0,2	0,21	0,4	5[b]	180	75
PS89-*b*-PFSF4	II, III	0,4	0,7	0,07	0,17	3[b]	180	76
PS28-*b*-PEMS2	II	0,9	0,2	0,14	0,17	5[b]	180	49
PS89-*b*-PEMS2	II	0,5	0,07	0,07	0,23	5[b]	180	54
PS28-*b*-PFMA6	II, III	6,7	0,2	0,07	0,17	4[b]	60	17
PS89-*b*-PFMA11	II	3,4	0,07	0,07	0,12	3[b]	60	34
PS35-*b*-PFS35	II	10,3	0,14	0,14	0,22	5[a]	240	68
PS35-*b*-PFS49	II	5,2	0,14	0,14	0,22	5[a]	180	69
PS53-*b*-PFS35	II	5,2	0,09	0,09	0,18	5[a]	180	74
PS74-*b*-PFS74	III, IV	27	0,27	0,27	0,53	5[a]	240	84

PMDETA was used as ligand except with PEIMA-*b*-PFMA. [a]xylene, [b]anisole, [c]2,2'bipyridine.

Table 3. Molecular characteristics of block copolymers.

Polymer	Publication	M_nNMR (gmol-1)	M_nSEC (gmol-1)	PDI
PEIMA-*b*-PFMA	I	24000	11500	1,2
PS28-*b*-PFSF4	II	5500	4000	1,3
PS89-*b*-PFSF4	II, III	11900	11400	1,4
PS28-*b*-PEMS2	II	4100	4300	1,2
PS89-*b*-PEMS2	II	10500	10000	1,2
PS28-*b*-PFMA6	II, III	6100	3200	1,3
PS89-*b*-PFMA11	II	15200	9600	1,1
PS35-*b*-PFS35	II	10500	12000	1,3
PS35-*b*-PFS49	II	13200	16000	1,4
PS53-*b*-PFS35	II	12400	12000	1,3
PS74-*b*-PFS74	III, IV	22000	18000	1,25

3.2.4 MODIFICATION OF PS-B-PFS (III, IV)

The pentafluorostyrene units react with thiols in clickfashion.[26] Block copolymer PS74-*b*-PFS74 was reacted with two different thiols, thioglycolic acid and 2,3,4,6-tetra-O-acetyl-1-thio-β-D-glucopyranose (SH-GlcAc4) (Scheme 5).

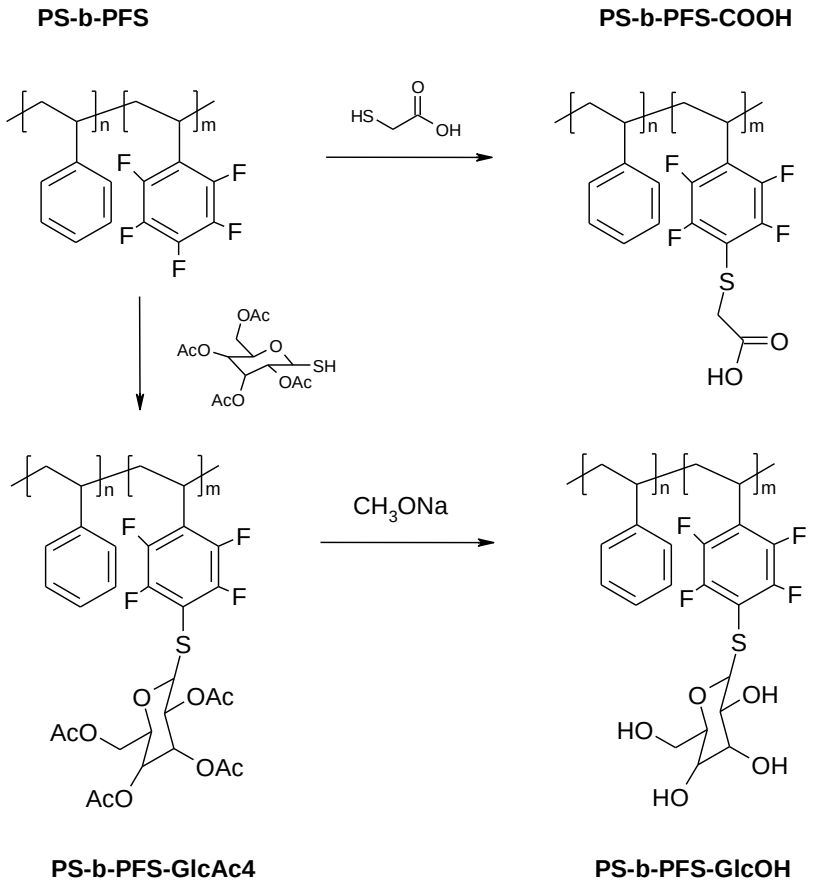

Scheme 5. Modification of the PS-*b*-PFS with thiols. Adapted with permission from Publication III. © 2014 Wiley Periodicals, Inc.

Successful reactions were ascertained by ^{1}H NMR and ^{19}F NMR. In the case of SH-GlcAc4 the deprotection of the acetyl groups of PS-*b*-PFS-GlcAc4 was monitored by ^{1}H NMR and IR.

3.3 ELECTROSPINNING OF FLUORINATED BLOCK COPOLYMERS (II)

PS35-*b*-PFS35, PS28-*b*-PFSF4 and PS89-*b*-PFMA11 were used in electrospinning. Chloroform was used as solvent with polymer concentration of 30% w/v. Mixtures of fluorinated block copolymer solutions and polystyrene (20% w/v) with M_n=123000 gmol^{-1} were also electrospun. All experiments were made using aluminum foil as the substrate.

3.4 BREATH FIGURE TEMPLATING (III)

Polymers were dissolved in chloroform with polymer concentrations from 1 to 100 gl^{-1}. Microscope glass slides were cleaned with Piranha solution before they were placed in humid environment (relative humidity, RH, 85%) and humid airflow was provided by bubbling air (2 $lmin^{-1}$) through a water vessel and directing the flow through an inverted funnel. 5 µl of the polymer solution was injected on the glass slides and the solvent allowed to evaporate. For stripping the outermost polymer layer to expose the underlying structure an adhesive tape was applied on the film and removed. As the deprotected PS-*b*-PFS-GlcOH polymer was poorly soluble in chloroform, glycopolymer films were made from the acetonide protected intermediate polymer, PS-*b*-PFS-GlcAc4, and the deprotection of the sugar residues was done after the film formation. The deprotection was carried out by immersing the BF films in methanol solution containing sodium methanolate for 2 h followed by washing with deionized water and drying at room temperature.

3.5 PREPARATION OF FLUORINATED NANOPARTICLES (IV)

Nanoparticles were prepared by three different methods, see Scheme 6.

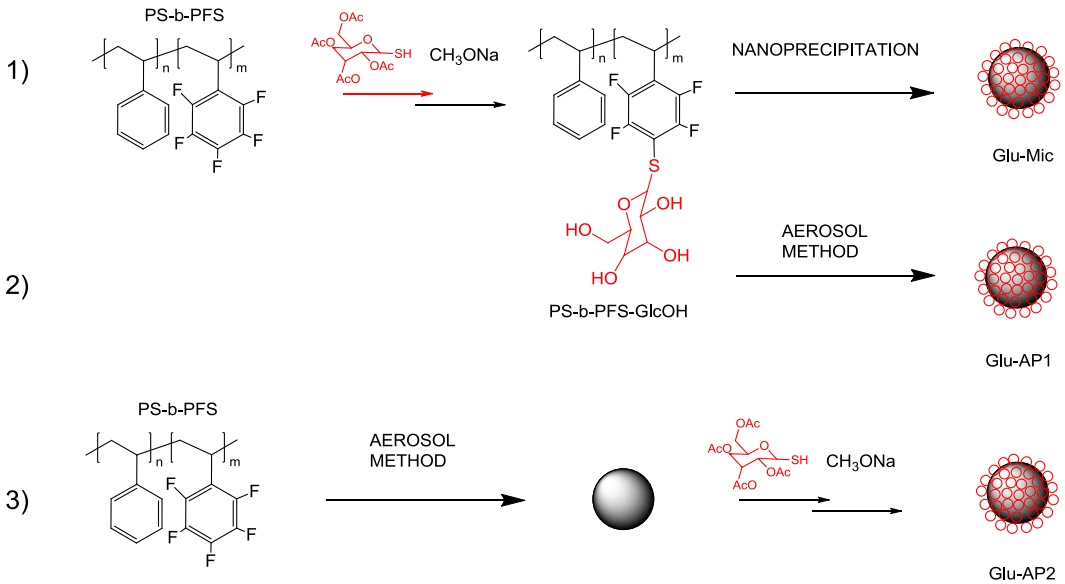

Scheme 6. Particle preparation pathways shown schematically. Adapted with permission from Publication IV. © 2014 Elsevier Ltd.

3.5.1 MICELLIZATION OF PS-B-PFS-GLCOH (IV)

PS-*b*-PFS-GlcOH in DMF with concentration of 2 gl^{-1} was titrated with distilled water until the solution turned turbid. The solution was dialysed

against distilled water for one week yielding glycomicelles, Glu-Mic with concentration of 1.0 gl^{-1}.

3.5.2 PREPARATION OF NANOPARTICLES VIA AEROSOL TECHNIQUE (IV)

The nanoparticles were produced from PS-*b*-PFS-GlcOH and PS-*b*-PFS 1 wt% DMF precursor solution using an aerosol reactor.[141,142] The particles were then dispersed in methanol-water mixture 1:1 v/v and dialyzed against distilled water for one week, yielding aerosol particles, Glu-AP1 with concentration of 0.1 gl^{-1}, determinated gravimetrically.

In order to make glycosylated nanoparticles, PS-*b*-PFS aerosol nanoparticles were dispersed in methanol (concentration 1 gl^{-1}) and reacted with SH-GlcAc4 in the presence of triethylamine for 18 h, followed by deprotection with sodium methanolate. The solution were then titrated with distilled water and dialyzed against distilled water for one week, yielding aerosol particles, Glu-AP2. Polymer concentration of the dispersion was adjusted to 0.1 gl^{-1}.

3.5.3 GLUCOSE QUANTIFICATION (IV)

The amounts of glucose on the nanoparticles were quantified by the anthrone-sulfuric acid method.[143] For glucose detachment from nanoparticles the dispersions were treated with 2 M HCl at 80 °C for 24 h. Solutions were then filtered to remove the precipitated polymer nanoparticles. The glucose solutions were treated with anthrone/H_2SO_4, kept at 100 °C for 10 minutes and the optical densities of solutions measured. The amount of glucose was determined by comparing the absorbance to standard glucose solutions treated with the same procedure.

3.5.4 RHODAMINE LABELLING OF GLYCOSYLATED NANOPARTICLES (IV)

In order to label the nanoparticles with rhodamine isothiocyanate (RITC) 17.8 µl of aqueous RITC solution (concentration 0.1 gl^{-1}) was added to a 200 µl aqueous polymer solution (concentration 0.1 gl^{-1}) and allowed to react at room temperature for 2 h.

3.6 INSTRUMENTATION

Size exclusion chromatography (SEC) was used to measure molar masses and molar mass size distributions of polymers. SEC was performed with Waters SEC chromatograph equipped with Styragel columns, and a 410 differential refractometer (Waters Instruments, Rochester, MN).

NMR analyses were conducted with Varian Gemini 2000 200 MHz, Varian UNITYINOVA 300 MHz or Bruker Avance III 500 MHz spectrometers.

Differential scanning calorimetry (DSC) measurements were performed with a Mettler 822e DSC under nitrogen atmosphere.

Surface tensions were measured either by a KSV Sigma with duNouy ring or by analyzing pendant drops using KSV CAM 200 instrument. Contact angle studies were done with a KSV CAM200 instrument.

A Brookhaven Instruments BI-200SM goniometer and a BI-9000AT digital correlator and Ar laser (LEXEL 85 l =488 or 514,5 nm) as light source were used for dynamic (DLS) and static light scattering (SLS). Specific refractive index increment (dn/dc) was measured with an Abbe 60/ED high precision refractometer (Bellingham and Stanley Ltd.) at a wavelength of 488 or 514,5 nm.

Transmission (TEM) and Scanning electron microscopy (SEM) as well as element mapping using energy dispersive spectroscopy (EDS) measurements were done with a Hitachi S-4800 field emission scanning microscope. Cryo-transmission electron microscopy was done by using Cryo-TEM, JEM-3200FSC, JEOL, Tokyo, Japan.

Atomic force microscopy (AFM) was carried out with a NTEGRA Prima (NT-MDT, Russia) atomic force microscope for analyzing the topography of the samples. AFM images were processed and analyzed with the Scanning Probe Image Processor software (SPIPTM, Image Metrology, Denmark).

Confocal laser scanning microscopy measurements were done by using a Leica TCS SP5 confocal laser scanning system with Leica DM5000 upright microscope, HCX APO 63x/1.30 Corr (glycerol) CS 21 objective and DD 488/561 beam splitter. Slice images were constructed with Imaris 7.6 software (Bitplane) without deconvolution.

IR measurements were carried out with a Bruker Alpha ATR-FTIR instrument.
Fluorescence studies were conducted with a Horiba Jobin Yvon Fluoromax-4 spectrofluorometer. For the determination of optical densities a Shimadzu

UV-1601PC UV/vis spectrometer was employed by monitoring the absorbance at 620 nm.

Electrospinning device consisted of a syringe infusion pump, a positively charged stainless steel HPLC capillary (0.51 mm ID, 1.59 mm OD, Supelco), and a negatively charged collector. Stainless steel plate covered with aluminium foil was used as the collector. The +15 kV positive charge was achieved with Spellman SL30P30/220 high voltage generator (Spellman High Voltage Electronics Corp.) with a low current output (limited to a few mA). -5 kV negative charge on the collector was achieved with Philip Harris 15kV high voltage generator (Philip Harris Ltd.) The polymer solution was delivered to metal capillary via a syringe pump (KDS-100-CE) with flow rate of 1 mlh^{-1}. The distance between blunt-end capillary and collector was 25 cm.

For aerosol a Collison-type atomizer was operated in recycling mode to atomize the precursor solution into aerosol droplets, which were carried into a heated reactor tube at 180 °C by a nitrogen carrier gas flowing at 2.5 gl^{-1}. Before collection, the aerosol nitrogen mixture was diluted and cooled with excess nitrogen flowing at 30 $lmin^{-1}$. The nanoparticles were collected size-selectively on aluminium foils using a Berner-type low pressure impactor.

4 RESULTS AND DISCUSSION

4.1 POLYMER SYNTHESIS

Synthesis and characterization of fluorinated polymers is challenging due to the fact that they often have limited solubility in common organic solvents. Copolymerization of fluorinated monomers with nonfluorinated ones is a viable methodology to improve their solubility without sacrificing the beneficial properties, *e.g.* surface activity.

4.1.1 RANDOM COPOLYMERIZATIONS (I)

In radical polymerizations of EIMA and FMA good reaction yields were obtained. Polydispersities were reasonable and the correlation of monomer feed ratio to the resulting polymer composition was good as can be seen from Table 1. No precipitation was observed during the copolymerizations while attempts to synthesise PFMA homopolymers lead to precipitation. The accurate determination of molar masses of semifluorinated polymers with SEC is problematic due to the solubility issues. The molar mass values obtained in the present study for the copolymers using commercial PMMA standards are smaller than the expected M_n of the copolymers. Reason for this is the fact that the eluent THF is a poorer solvent for semifluorinated copolymers than for PMMA. Semifluorinated copolymers therefore have compact conformation in THF which leads to smaller hydrodynamic radius and longer elution times compared with the standards used. When the fluorine content increases the solubilities and the hydrodynamic sizes decrease further. This explains why the observed M_n of P(EIMA-FMA)-60% is much lower than in the case of other copolymers measured under identical conditions. Fluorine content of copolymers was determined with ^{1}H NMR by comparing the integrals of the methylene protons (3.9 ppm) next to the ester moiety of EIMA and methylene protons next to the ester moiety of fluorinated monomer (4.2 ppm). In some cases addition of hexafluorobenzene to $CDCl_3$ was required to break up possible micelles of the copolymers and to get improved signals for protons of fluorinated repeating units as shown Figure 1.

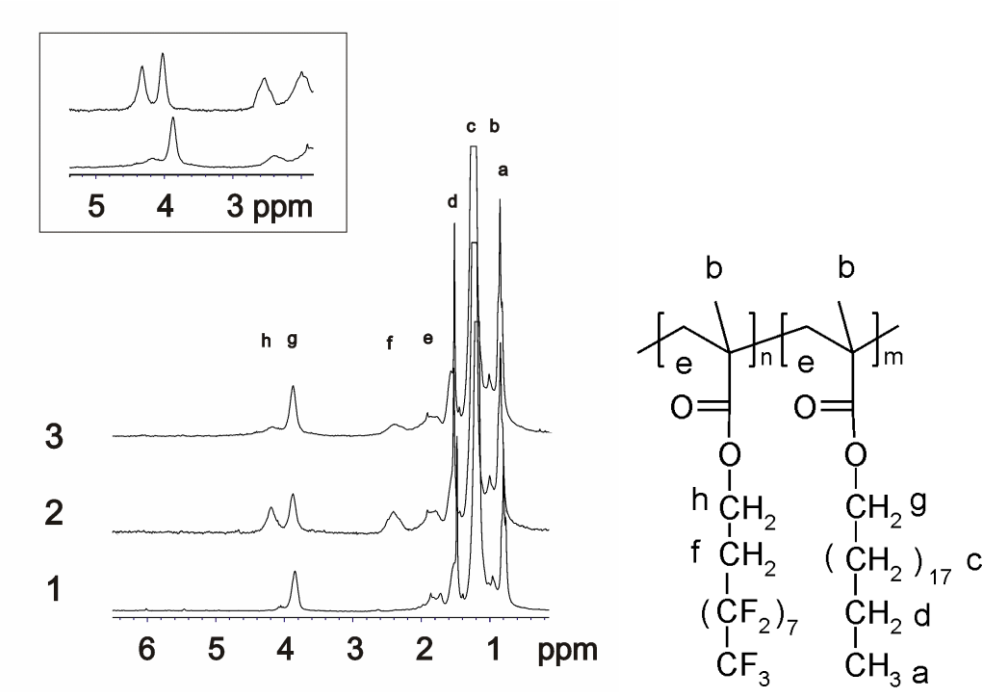

Figure 1. Chemical structures of copolymers and 1H NMR spectra of the polymers in $CDCl_3$. 1. P(EIMA), 2. P(EIMA-FMA)-50%, and 3. PEIMA-*b*-PFMA. Inset shows the 1H NMR spectra of PEIMA-*b*-PFMA in $CDCl_3$ (bottom) and $CDCl_3$/hexafluorobenzene (top). Adapted with permission from Publication I. © 2008 John Wiley & Sons, Ltd.

4.1.2 ESTIMATION OF THE REACTIVITY RATIOS (I)

In order to estimate monomer reactivity ratios the copolymerization of EIMA and FMA were performed in NMR tubes and followed online with ^{1}H NMR.

To assess the reactivity ratios of the monomers Fineman-Ross (F-R) and Kelen-Tüdős (K-T) methods were employed. Figures 2 and 3 show the Fineman-Ross and Kelen-Tüdős plots, respectively, for the P(FMA-EIMA) copolymers and Table 4 summarizes the F-R and K-T parameters resulting from the analysis. The reactivity ratios of the FMA (r_a) and EIMA (r_b), respectively, determined by these two methods are summarized in Table 5.

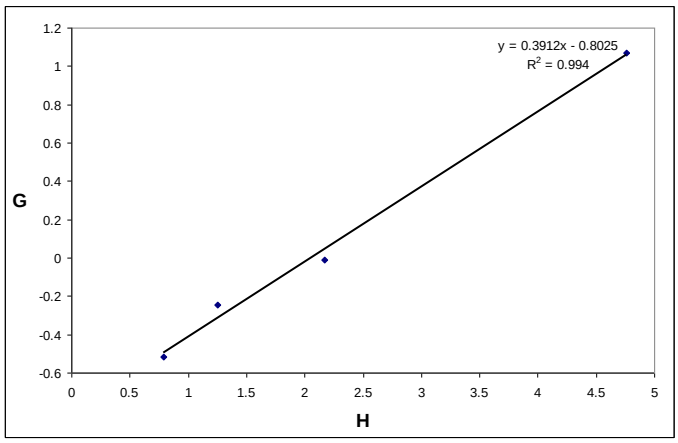

Figure 2. Fineman-Ross plot for FMA and EIMA copolymer.

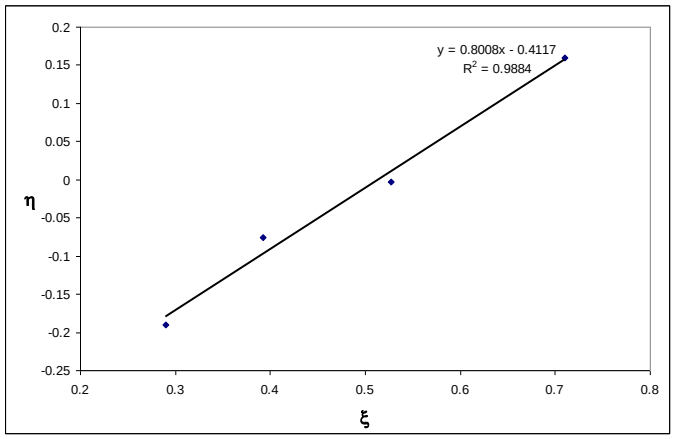

Figure 3. Kelen-Tüdős plot for FMA and EIMA copolymer.

Table 4. F-R and K-T parameters obtained by data analysis.

			x			X			G	H	η	ξ	α
	f_a	f_b	f_a/f_b	F_a	F_b	F_a/F_b	X/x^2	(X-1)/x	x(X-1)/X	x^2/X	G/(H+ α)	H/(H+ α)	
1	0,74	0,26	2,78	0,62	0,38	1,63	0,21	0,22	1,07	4,76	0,16	0,71	1,94
2	0,59	0,41	1,47	0,5	0,5	0,99	0,46	-0,01	-0,01	2,17	0	0,53	1,94
3	0,4	0,6	0,67	0,36	0,64	0,56	1,26	-0,66	-0,52	0,79	-0,19	0,29	1,94
4	0,5	0,5	1	0,45	0,55	0,8	0,8	-0,19	-0,24	1,25	-0,08	0,39	1,94

Table 5. Reactivity ratios for copolymer of FMA and EIMA. Adapted with permission from Publication I. © 2008 John Wiley & Sons, Ltd.

Copolymer	Method	r_a	r_b	r_a*r_b	Nature of copolymer sequence
P(FMA-EIMA)	Kelen-Tüdős	0,39	0,79	0,31	Tendency to alternate
	Fineman-Ross	0,39	0,8	0,31	

Linear fits and very similar results were obtained using both methods. The reactivity ratios r_a and r_b of both monomers were found to be less than 1 and $r_a r_b$= 0.31 from both K-T and F-R analyses. This indicates that the resulting copolymers are not completely random since r_b is not very much larger than r_a. Rather the copolymers are likely to have a tendency to alternate, favouring longer blocks of EIMA monomers in the chain due to the higher value of r_b compared with r_a. The reactivity ratio obtained for EIMA is somewhat low compared with those obtained for a series of copolymers using acrylates with different side chain length[41] where increasing reactivity ratios for the non-fluorinated acrylate were observed with increasing aliphatic side chain length and for the longest chain, n=18, the reactivity ratio was over 2. These conflicting results may be explained by the different solvent that used by Morita *et al.*[41] and also due to the different method used in obtaining the reactivity ratios. However, Morita *et al.*[41] similarly concluded that for acrylates with different side chain lengths somewhat alternating random copolymers are obtained by copolymerization. Random copolymers with a tendency to alternate were also found in studies of copolymerizations of a fluorinated acrylate and styrene by Saïdi *et al.*[81] The somewhat alternating nature of the P(FMA-EIMA) copolymers found with reactivity ratio analysis are in accordance with the observed thermal behaviour, where the crystallinity of the fluorine part is diminished and the EIMA crystallinity decreases more than is expected with increasing FMA mass fraction, see Figure 4.

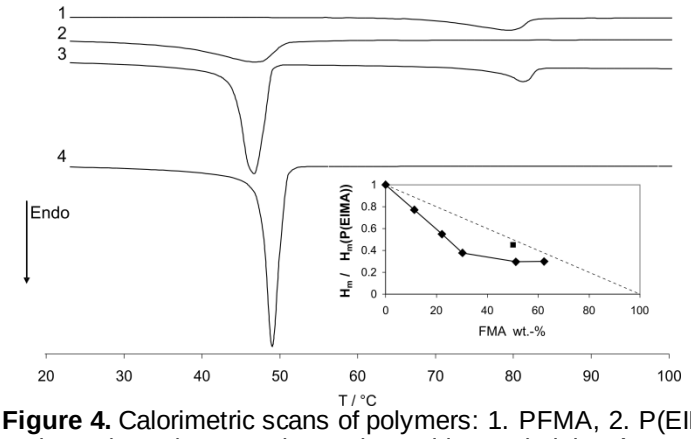

Figure 4. Calorimetric scans of polymers: 1. PFMA, 2. P(EIMA-FMA)-50%, 3. PEIMA-*b*-PFMA and 4. P(EIMA). Inset shows the melting enthalpies ΔHm of the P(EIMA-FMA) copolymers (♦) and PEIMA-*b*-PFMA block copolymer (■) divided by the melting enthalpy P(EIMA) homopolymer plotted against wt% of FMA. Straight dashed line shows linear decrease with wt% of FMA. Adapted with permission from Publication I. © 2008 John Wiley & Sons, Ltd.

4.1.3 ATRP POLYMERIZATIONS (I, II, III)

ATRP was selected as the method to build block copolymers. The idea was to first build up a macroinitiator from eicosanyl methacrylate or styrene. This was successfully done by using phenyl 2-bromoisobutyrate or phenyl 2-

bromopropionate as initiator. Decent polydispersities and expected molar masses (<10000 $gmol^{-1}$) were obtained.

The macroinitiators were used to polymerize fluorinated monomers shown in Scheme 4 and Tables 2 and 3. Structural characterization of fluorinated block polymers is often complicated by the tendency of the molecules to associate due to their fluorinated segments.[6] Monomodal SEC elution curves, Figure 5, were obtained for the products. Together with NMR signals from the fluorinated blocks, Figure 6, they enable the calculation of the number of fluorinated units in different block copolymers and estimation of the polydispersities of the products.

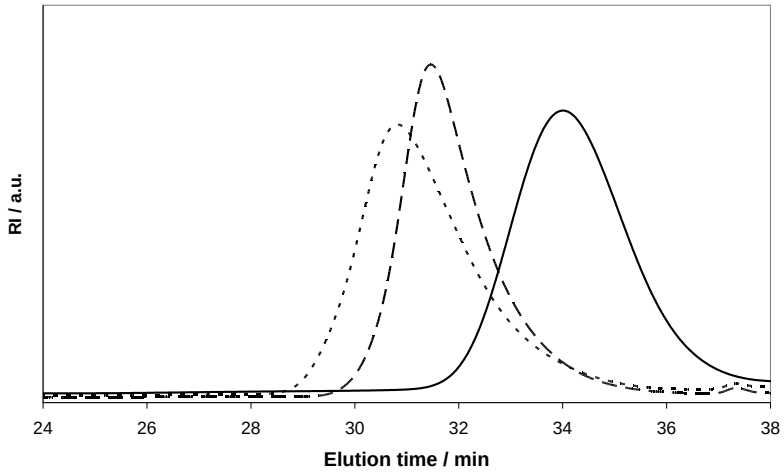

Figure 5. SEC elution chromatograms of PS35 (line), PS35-*b*-PFS35 (dashed line) and PS35-*b*-PFS49 (dotted line). Adapted with permission from Publication II. © 2009 Elsevier Ltd.

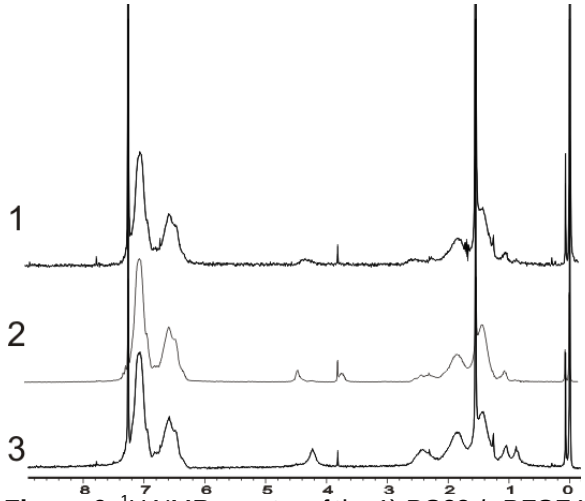

Figure 6. ^{1}H NMR spectra of the 1) PS28-*b*-PFSF4, 2) PS28-*b*-PEMS2 and 3) PS28-*b*-PFMA6. Adapted with permission from Publication II. © 2009 Elsevier Ltd.

As is evident from the Table 3 the polymers bearing fluorinated alkyl substituted monomers, EMS, FSF and FMA, have low degrees of

polymerization of the fluorinated block, only a few monomer units. This is most probably due to the conditions chosen for polymerization and to the bulkiness of the monomers. Nevertheless, the weight fraction of the fluorinated monomers is high compared to their degree of polymerization due to the high molar mass of the fluorinated monomers.

4.2 SURFACE ACTIVITY IN SOLUTION (I, II)

All toluene solutions of the copolymers showed a declining surface tension when polymer concentration was increased, while the P(EIMA) or PS homopolymer do not affect the surface tension of toluene in the studied concentration range. See Figures 7 and 8.

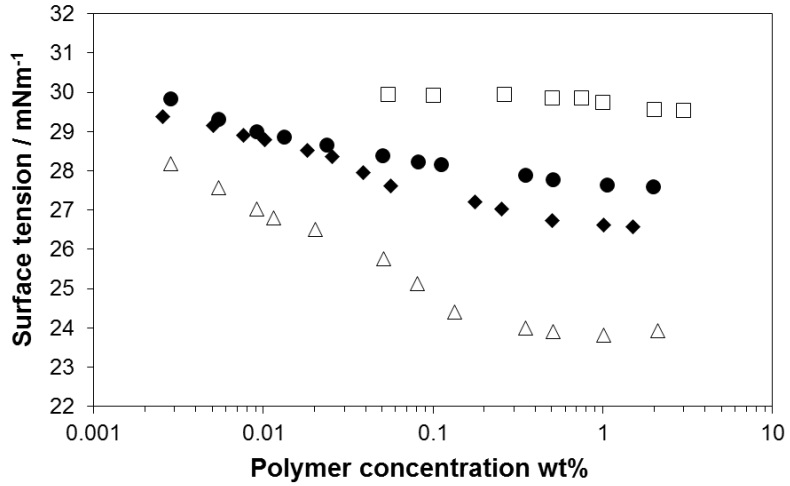

Figure 7. Surface tension as a function of P(EIMA-FMA) copolymers as function of polymer concentration in toluene. P(EIMA-FMA)-10% (□), P(EIMA-FMA)-30% (●), P(EIMA-FMA)-50% (△) and PEIMA-*b*-FMA (♦).

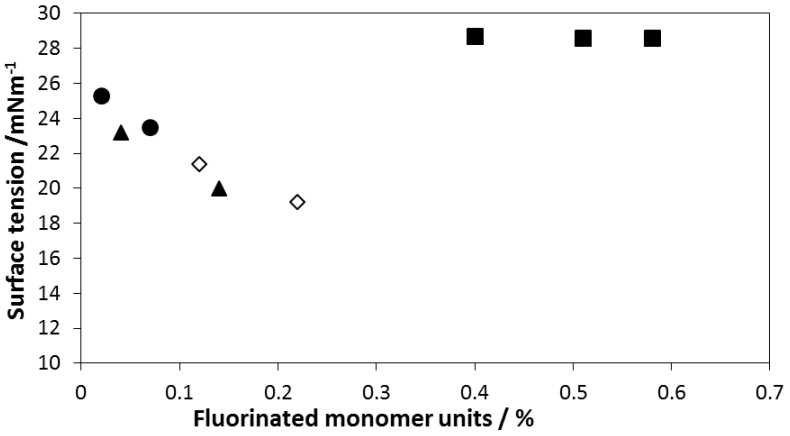

Figure 8. Surface tensions of 1 wt% the block copolymer solutions in toluene plotted against fraction of fluorinated monomers. PS-*b*-PFS (■),PS-*b*-PFSF(▲), PS-*b*-PEMS(●) and PS-*b*-PFMA (◊).

All PS-*b*-PFS polymers showed similar surface tensions regardless of the polymer composition in toluene. This shows that the effect of the lengths of PS macroinitiator or the fluorinated block is negligible on the resulting surface tension. The situation is different in the case of the polymers bearing fluorinated alkyl chains. They show a much more pronounced effect on the surface tension than the block copolymers based on poly(pentafluorostyrene), and also the fraction of fluorinated units has an effect. It can be seen from Figure 8, that the increasing fraction of fluorinated alkyl groups, especially the CF_3 groups, is responsible for the enhanced surface activity. The surface tensions found for PS-*b*-PFSF, PS-*b*-PEMS and PS-*b*-PFMA are comparable to the ones found for other fluorinated acrylate copolymers in toluene. For example, Krupers *et al.*[82] observed corresponding values for poly(methyl methacrylate)-*b*-poly(1H,1H,2H,2H-perfluorohexyl methacrylate) and poly(methyl methacrylate)-*b*-poly(1H,1H,2H,2H-perfluorooctylmethacrylate) copolymers.

4.3 ELECTROSPINNING (II)

In the electrostatic coating process with polystyrene, PS123, a mixture of nanofibers with diameter of 200-300 nm and particles with diameter around 10-20 μm was formed, see Figure 9 for scanning electron micrograph. The studied fluorinated block copolymers, PS35-*b*-PFS35, PS28-*b*-PFSF4 and PS89-*b*-PFMA11 electrospun as such formed 10-20 μm particles as shown in Figure 9, completely without the formation of nanofibers. This effect is most likely due to the rather low molar mass of the polymers and the aggregation tendency which result in insufficient viscosity and viscoelasticity. In all cases the polymer particles have a shape of shrunken spheres, which originates from the solvent-containing polymer spheres collapsing after the spinning process as chloroform evaporates.

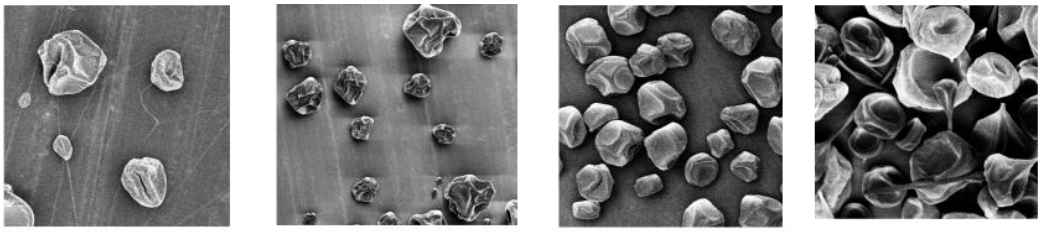

Figure 9. SEM micrographs (100 μm x 100 μm) of electrospun polymers. From left to right PS123, PS35-*b*-PFS35, PS89-*b*-PFMA11 and PS28-*b*-PFSF4. Adapted with permission from Publication II. © 2009 Elsevier Ltd.

Higher magnification of the surface of the fibers or particles in Figure 10, show holes of the order of tens of nanometers which have formed after the electrospinning process upon solvent drying.

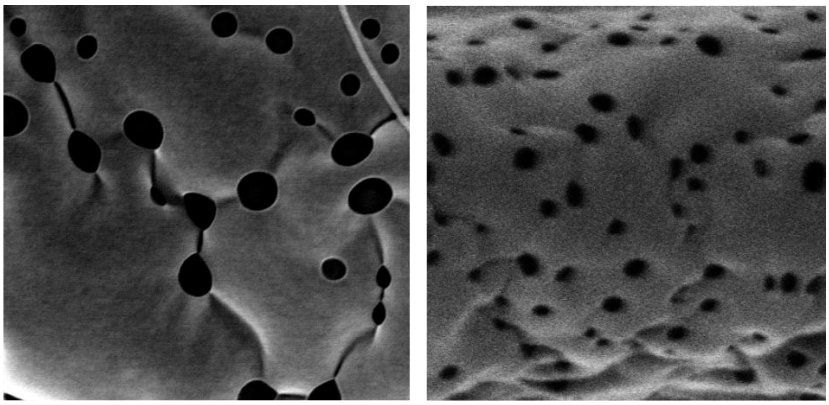

Figure 10. SEM micrographs (2 µm x 2 µm) of electrospun polymers PS123(left) and PS89-*b*-PFMA11 (right). Adapted with permission from Publication II. © 2009 Elsevier Ltd.

Due to the relatively high price of fluorinated compounds it would be very economical if the amount of fluorinated materials could be lowered without compromising the properties. We chose to use mixed solutions of PS123 and fluorinated block copolymers for further electrospinning experiments. Similar collapsed spheres as in the case of fluorinated block copolymers were formed, but also nanofibers with a diameter of 200-300 nm were created, see Figure 11. The formation of nanofibers is caused by the higher molecular weight polystyrene component, which allows the chain entanglement in the whipping process during the electrospinning. However, as particles were formed also during the electrospinning of PS123 itself and the electron micrographs resemble very much those of pure PS123, we conclude that mixing the fluorinated block copolymer did not change the behavior of the PS123 in the electrospinning process.

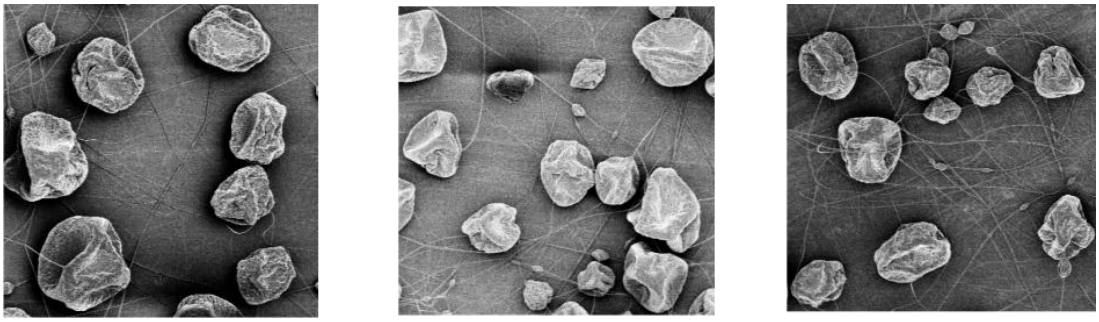

Figure 11. SEM micrographs (100 µm x 100 µm) of electrospun polymer mixtures of PS123 containing 10 wt% fluorinated polymer. From left to right PS35-*b*-PFS35, PS89-*b*-PFMA11 and PS28-*b*-PFSF4. Adapted with permission from Publication II. © 2009 Elsevier Ltd.

4.4 GLYCOSYLATION OF PS-B-PFS (III, IV)

The modification of the pentafluorostyrene units of PS-*b*-PFS was performed with 2,3,4,6-tetra-O-acetyl-1-thio-β-D-glucopyranose (SH-GlcAc4), shown in Scheme 5. ^{1}H NMR spectra show the appearance of the acetylated glucose units in the ^{1}H NMR of PS-*b*-PFS-GlcAc4 and the success of the deprotection

of the acetyl groups in the spectra of PS-*b*-PFS-GlcOH at 2 ppm as shown in Figure 12. ^{19}F NMR spectra of the PS-*b*-PFS and PS-*b*-PFS-GlcAc4 confirm the substitution of the para-fluorine position in pentafluorostyrene units to ~ 90%, Figure 13.

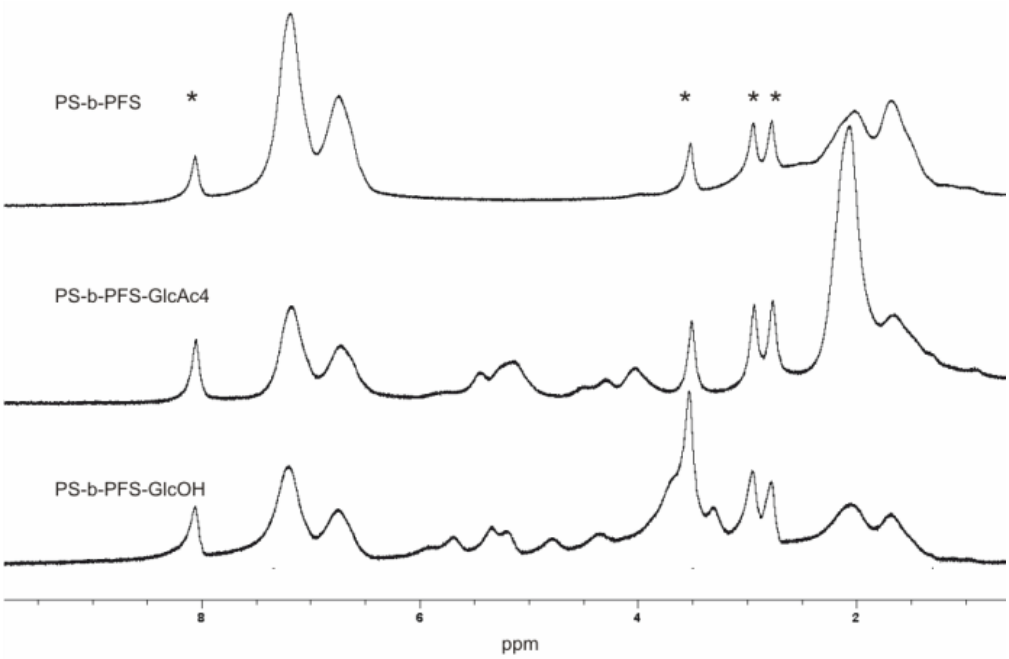

Figure 12. 1H NMR spectra (DMF-d_6) of PS-*b*-PFS, acetylated PS-*b*-PFS-GlcAc4 and PS-*b*-PFS-GlcOH. The solvent signals are marked with asterisk. Adapted with permission from Publication IV. © 2014 Elsevier Ltd.

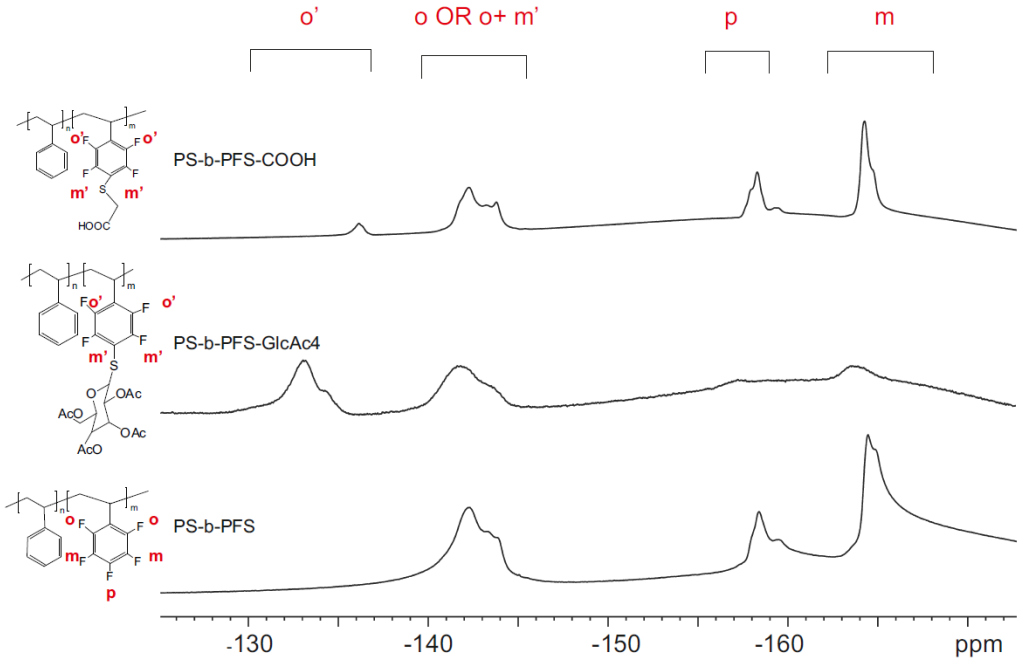

Figure 13. ^{19}F NMR spectra of PS-*b*-PFS-COOH, PS-*b*-PFS-GlcAc4 and PS-*b*-PFS. Adapted with permission from Publication III. © 2014 Wiley Periodicals, Inc.

4.5 NANOPARTICLE PREPARATION (IV)

Three different routes were selected to make glucose functionalized nanoparticles, Scheme 6. These routes were nanoprecipitation and aerosol preparation of two different polymers. In the nanoprecipitation the PS-*b*-PFS-GlcOH was dissolved in DMF and the Glu-Mic particles were formed upon addition of water. In the aerosol method either PS-*b*-PFS or PS-*b*-PFS-GlcOH were dissolved in DMF and particles formed in gas phase in the aerosol reactor. The method yields dry particles which can be dispersed in a desired solvent. Glycosylated nanoparticles, Glu-AP1 were formed from the aerosol processing of PS-*b*-PFS-GlcOH while aerosol processing of PS-*b*-PFS yields "naked" fluorinated nanoparticles. The latter particles were further glycosylated with SH-GlcAc4 from the surface and further deprotected, Glu-AP2. In the case of Glu-AP2, the water dispersibility gave a direct proof of the successful glycosylation.

Figure 14 presents TEM images of the particles and it can be observed that the particles are spherical in all cases. When the particles are dispersed in water, they can be observed by DLS, see Figure 15, showing that all have narrow size distributions but different particle sizes depending on the preparation method. Table 6 collects the data of the particle sizes by DLS and cryo-TEM.

Table 6. Particle sizes from dynamic light scattering and TEM analysis and the glucose concentrations on the surfaces of the particles. Adapted with permission from Publication IV. © 2014 Elsevier Ltd.

Sample	Preparation method	Diameter (DLS) nm	Diameter (TEM) nm n=30	Glucose concentration $moll^{-1a}$
Glu-Mic	Titration	97 ± 2	69 ± 10	2.22E-07
Glu-AP1	Aerosol	357 ±10	289 ± 60	1.49E-07
Glu-AP2	Postfunctionalization of PS-b-PFS aerosol particles	194 ± 10	268 ± 46[b]	1.13E-07

[a] For a 1 gl^{-1} nanoparticle solution. Determined via the anthron sulfuric acid method.

[b] Measured for PS-b-PFS aerosol particles

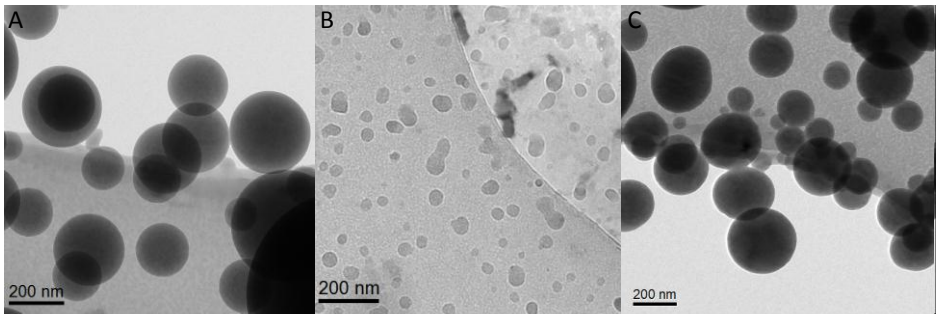

Figure 14. Cryo-TEM images of the particles. A) PS-b-PFS, B) Glu-Mic and C) Glu-AP1. Adapted with permission from Publication IV. © 2014 Elsevier Ltd.

Smallest sizes were observed for the particles prepared by nanoprecipitation, with average diameter of 97 nm according to DLS. The particles prepared by aerosol technique have significantly larger mean diameters, Glu-AP1 357 nm and Glu-AP2 194 nm. The difference between the two types of aerosol particles is likely to result from the different interfacial activity of the non-glycosylated and glycosylated polymers in aerosol reactor, respectively.

The amount of glucose units on surfaces of nanoparticles was measured. Firstly the water dispersions were treated with HCl to detach glucose units from the surface of nanoparticles. After filtrating solid nanoparticles from the solution, anthron-sulphuric acid solution was reacted with detached glucose giving dark green colors in solutions. The optical densities were then measured with UV-vis spectrometer and compared with similarly treated standard glucose solutions, resulting in glucose concentrations shown in Table 6.

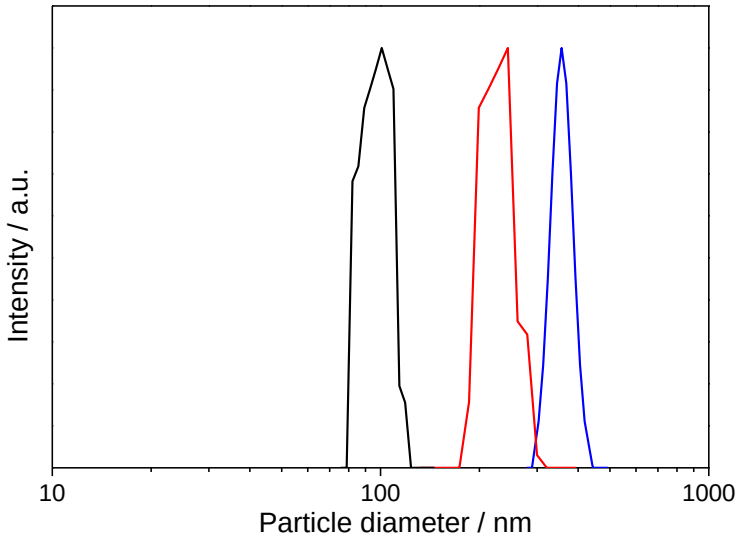

Figure 15. Size distributions of Glu-Mic prepared by nanoprecipitation (black), aerosol particles Glu-AP1 (blue) and aerosol particles Glu-AP2 (red). Adapted with permission from Publication IV.

4.6 BREATH FIGURE FORMATION (III)

After finding successful experimental conditions for porous breath figure formation from the solutions other experimental parameters were kept constant but the effect of polymer concentration was studied. SEM analyses of the BF films made with different polymer concentrations reveal that the polymer concentration plays a significant role. If the polymer concentration was below 50 gl^{-1}, regular breath figures were obtained only on rather small areas together with large disordered or flat areas. In the case of polymer

concentration of 50 gl^{-1} or more, large areas containing pores were formed, see Figure 16 and Table 7. For the hydrophobic fluorinated copolymers, the higher the polymer concentration was, the smaller pores were obtained. At the same time the pore size distribution became narrower. This is explained by the effect of increased polymer concentration that stops the growth of the water droplets at an earlier stage and leads to the formation of smaller pores. This is in agreement with previous reports,[120] where the pore size has been found to be inversely dependent on the concentration and the size distribution has also narrowed with polymer concentration.

Table 7. Average pore sizes from SEM and AFM analysis from films with different casting conditions. Adapted with permission from Publication III. © 2014 Wiley Periodicals, Inc.

Solution	Average pore size / µm				
	PS89-*b*-PFSF4	PS28-*b*-PFMA6	PS74-*b*-PFS74	PS-*b*-PFS-GlcOH[a]	PS-*b*-PFS-COOH[a]
$CHCl_3$ 50 gl^{-1}	0,72	1,34	1,26/1,45	1,2	0,2-0,7
$CHCl_3$ 100 gl^{-1}	0,67	0,43	0,63	-	-

[a]Values from AFM analysis.

.

A cross-sectional SEM image, Figure 17, of the PS74-*b*-PFS74 film reveals that the pores do not extend to the bottom of the film, but instead are formed by condensation of water droplets in the top layer, leaving a solid non-porous polymer film beneath the porous structure. This is explained by the higher density of chloroform used as a solvent compared to that of water acting as the pore forming agent. The SEM image also reveals that the porous surface layer is supported by pillar-like structures forming the pore walls. The depth of the pores was found to be roughly 1.7 µm and the diameter of the underlying pores observed from the side is ~3 µm compared with average pore diameter of 1.26 µm observed on the surface.

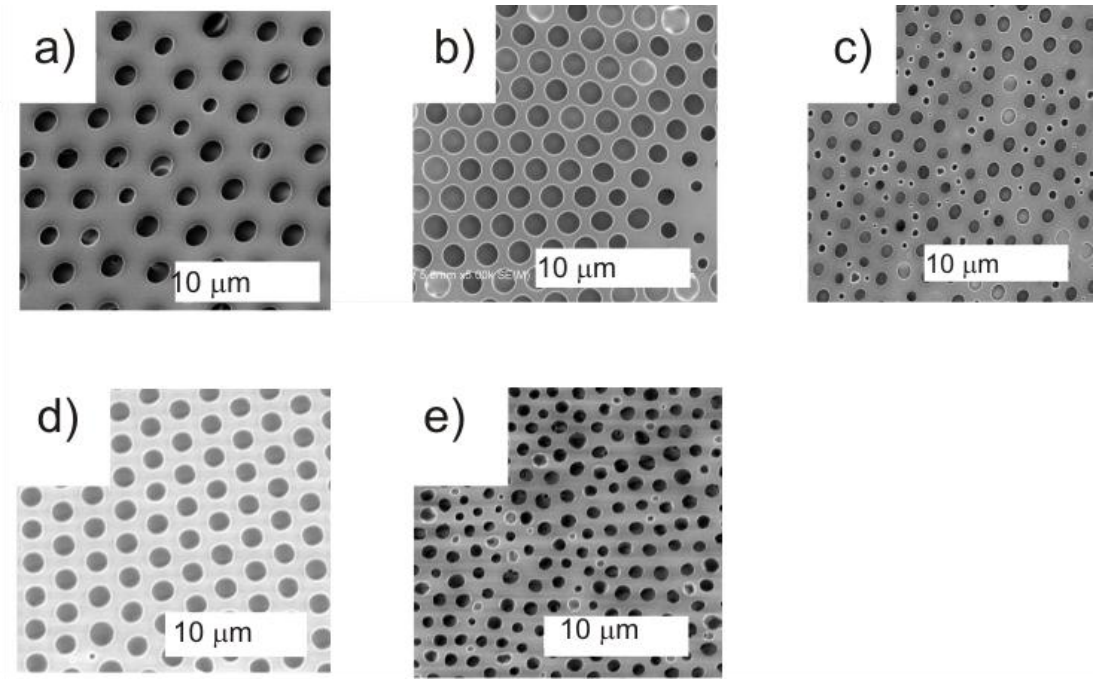

Figure 16. Scanning electron micrographs of breath figure films of PS74-*b*-PFS74 (a), PS28-*b*-PFMA6 (b), PS89-*b*-PFSF4 (c), PS-*b*-PFS-GlcAc4 (d) and PS-*b*-PFS-COOH (e). Polymer concentrations 50 gl^{-1} in CHCl3. Adapted with permission from Publication III. © 2014 Wiley Periodicals, Inc.

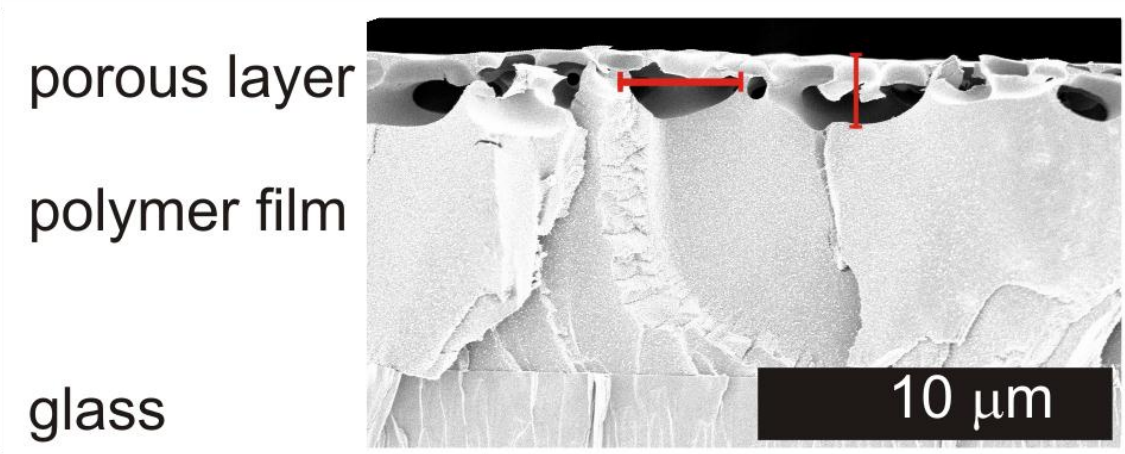

Figure 17. Cross-sectional SEM image of PS74-*b*-PFS74 BF film with scale bars indicating the depth and diameter of the pores. Polymer concentration 50 gl^{-1} in $CHCl_3$. Adapted with permission from Publication III. © 2014 Wiley Periodicals, Inc.

Due to the fact that PS-*b*-PFS-GlcOH is not fully soluble in $CHCl_3$ in the studied concentration range, BF films were made of PS-*b*-PFS-GlcAc4 and then the hydroxyl groups at the surface were deprotected to yield PS-b-PFS-GlcOH films. Successful deprotection was confirmed by IR measurements that show the disappearance of the acetyl groups, see Figure 18.

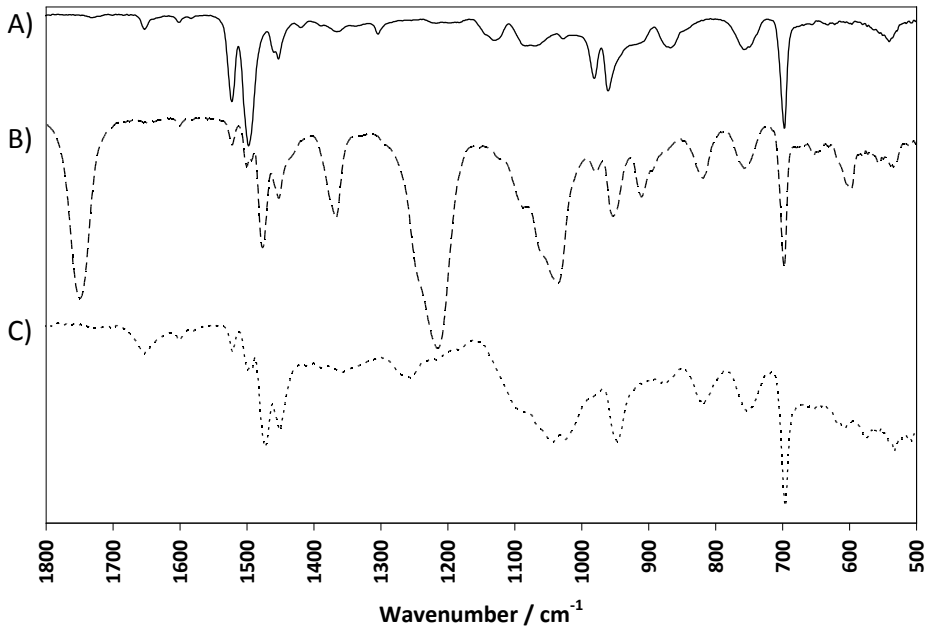

Figure 18. IR spectra of BF films of PS74-*b*-PFS74 (A), PS-*b*-PFS-GlcAc4 (B) and PS-*b*-PFS-GlcOH (C). Adapted with permission from Publication III. © 2014 Wiley Periodicals, Inc.

The BF films of PS-*b*-PFS-GlcAc4 and PS-*b*-PFS-COOH, respectively, made from 50 gL^{-1} chloroform solutions have also porous structures as shown in AFM analysis in Figure 19. It can also be clearly seen that in PS-*b*-PFS-GlcOH (Figure 22b) the porous structure is retained.

AFM analyses also indicate that the average sizes of the pores in the PS-*b*-PFS-GlcOH BF film (~1.2 μm) are slightly smaller than for the corresponding PS74-*b*-PFS74 (1.45 μm). Further, the PS-*b*-PFS-COOH BF film shows smaller pores compared with the other two. This can be explained by the fact that with increasing the hydrophilicity of the block the polymer does not stabilize water droplets so efficiently leading to the loss of the regular pore structure. This phenomenon has been observed in the case of polystyrene-block-poly(N,N-dimethylacrylamide) polymers.[144] Also in the case of amphiphilic graft copolymers PS-*g*-PEO the increase in the PEO content led to sponge-like structured membranes and the polymers with the lowest PEO content produced regular porous membranes.[145] The PS-*b*-PFS-COOH is more hydrophilic than the PS-*b*-PFS-GlcAc4 leading to the observed pore size decrease. The observed pore depths from AFM analyses (PS74-*b*-PFS74 1.4 μm, PS-*b*-PFS-GlcOH 1.2 μm) correspond well to the observed surface pore diameter as shown in Figure 17.

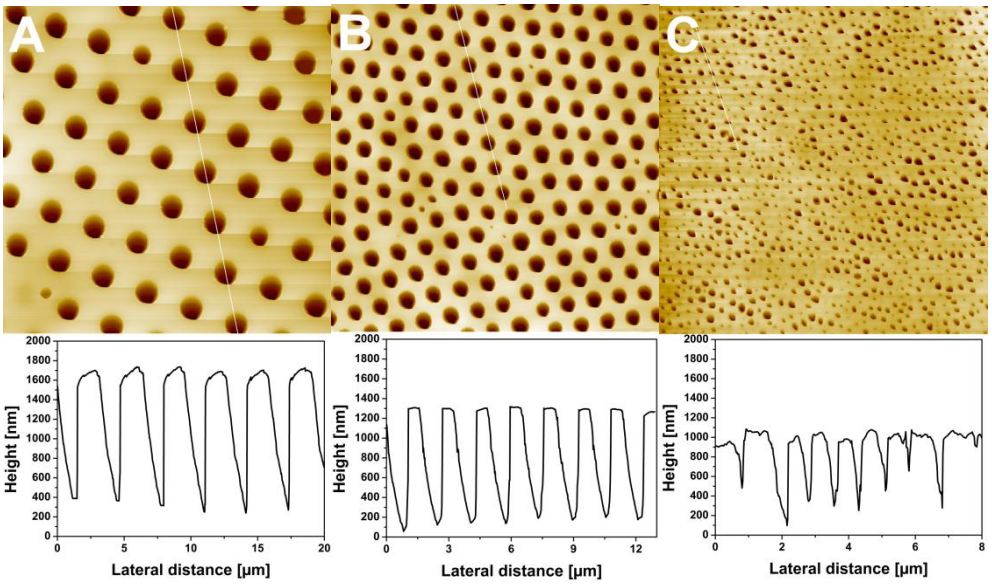

Figure 19. AFM topographs (image size 20 µm × 20 µm) of (A) PS74-*b*-PFS74 (height scale 2 µm), (B) PS-*b*-PFS-GlcOH(height scale 1.5 µm) and (C) PS-*b*-PFS-COOH (height scale 1.2 µm). Also shown are line profiles for respective samples over the porous structure. Adapted with permission from Publication III. © 2014 Wiley Periodicals, Inc.

4.7 CONTACT ANGLE STUDIES (II, III)

Depending on the fluorinated monomer used and the deposition technique, see Figure 20, fluorinated block copolymers have very different surface characteristics. The most hydrophobic surfaces are formed by electrospinning using the polymers based on CF_3 containing monomers, PS28-*b*-PFSF4 and PS89-*b*-PFMA11. Both polymers exhibit a contact angle above 150°. The solvent casted films of these polymers have smaller contact angles, of the order of 115-120°. In the case of the electrospun block copolymer having poly(pentafluorostyrene) block, PS35-*b*-PFS35, enhanced hydrophobicity was not observed when compared with the solvent casted sample. Therefore it can be stated that in addition to surface roughness, the enrichment of the CF_3 groups in to the polymer surface is responsible for the enhanced hydrophobicity.

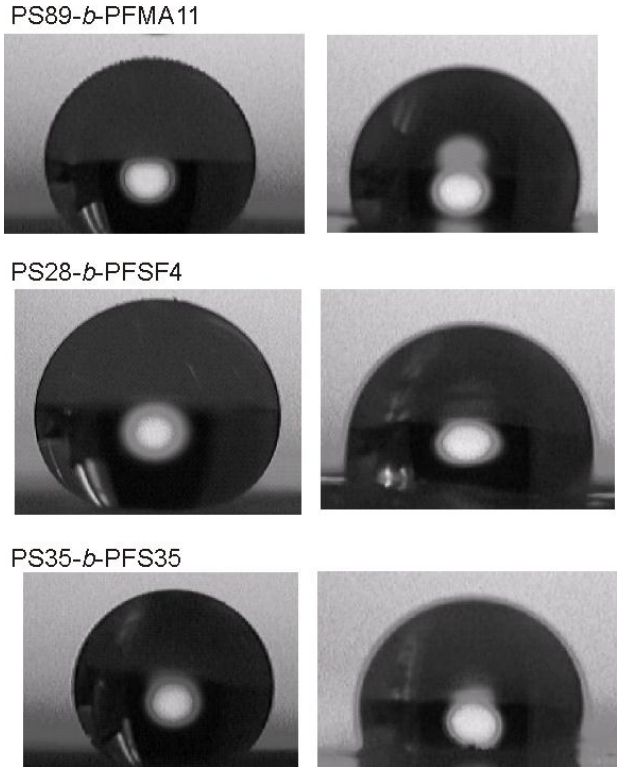

Figure 20. Photographs of water droplets on electrospun materials (left) and solution casted surfaces (right) for different neat block copolymer solutions. Adapted with permission from Publication II. © 2009 Elsevier Ltd.

The known tendency of fluorinated units to enrich on the surface, encouraged us to electrospin materials containing only a fraction of fluorinated material, which would be beneficial also economically taking into account the high price of fluorinated materials. Polymer solutions containing fluorinated block copolymers were mixed with a solution of polystyrene with molecular weight of 123000 $gmol^{-1}$ as described in Chapter 3.3. Figure 21 shows how the concentration of the fluorinated block copolymer affects the contact angles of the electrospun surfaces. PS28-*b*-PFSF4 and PS89-*b*-PFMA11 retained the surface hydrophobicity to a large degree even when the amount of fluorinated block copolymers decreased to 10 wt%. The practical implication is that the amount of the fluorinated compound can be reduced significantly while retaining the properties, thus making the use of these materials more commercially viable.

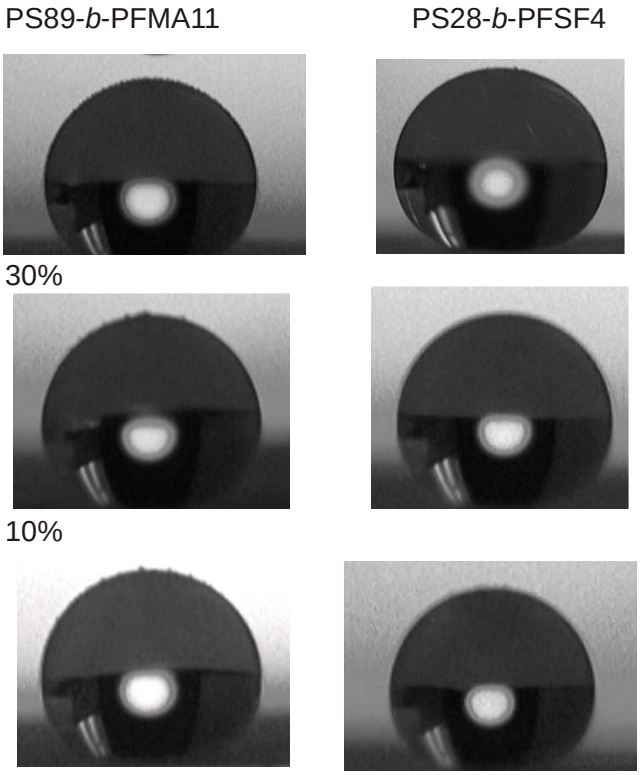

Figure 21. Photographs of water droplets on electrospun mixed solutions of PS123 and fluorinated block copolymer with different block copolymer weight fractions (in wt% of block copolymer to PS123). Adapted with permission from Publication II. © 2009 Elsevier Ltd.

Unlike in electrospinning, in the breath figure technique water is usually used as the templating solvent. This makes the system very different compared with an electrospun surface, because water is used as a "mold" and it therefore could prevent the enrichment of hydrophobic fluorinated moieties on the surface. To examine the effect of the BF process on the surface properties of the block copolymers, contact angles of water (CA_{water}) and dodecane ($CA_{dodecane}$) were compared between flat surfaces made by solvent casting, BF films and tape stripped BF films. Table 8 collects the data of measured contact angles. As can be seen from the Table 8 the BF films without thioglycolic acid or glucose in general exhibit higher contact angles compared with solvent casted films and, more importantly, the CF_3 containing polymers have highest contact angles for both water and dodecane. It was observed that the presence of water in the BF templating does not significantly alter the enrichment of fluorinated moieties on the surface.

PS74-*b*-PFS74 BF films made from 50 or 100 gl^{-1} chloroform solutions have similar water contact angles indicating that the difference in pore sizes at this size range does not alter the contact angle. To increase the surface roughness film surface of the BF films was removed by tape stripping the surface. As shown in Table 8, tape peeled BF film surfaces show significantly increased CA_{water} compared with either flat films or unmodified BF films. The polymers having CF_3 groups, PS28-*b*-PFMA6 and PS89-*b*-PFSF4, somewhat

surprisingly show smaller increase in CA_{water} compared to PS74-*b*-PFS74. The different pillar structure of the peeled films is the explanation of the difference. As shown in Figures 17 and 22, the underlying pore structure of PS74-*b*-PFS74 consists of much larger pores and the increase in surface roughness is larger than in the case of the two other films. Consequently, the CA_{water} increases due to the increased roughness and the peeled PS28-*b*-PFMA6 and PS74-*b*-PFS74 films are superhydrophobic (CA_{water} >150 °). The $CA_{dodecane}$ is similarly affected by the chemical nature of the films, the CF_3 containing polymers having the highest $CA_{dodecane}$. However, for most of the peeled surfaces $CA_{dodecane}$ decreases compared with the BF films, which is due to the low surface tension of the dodecane that allows it to spread on the rough needle-like surfaces.

Table 8. Contact angle data for films with 50 gl^{-1} polymer concentration in $CHCl_3$. Adapted with permission from Publication III. © 2014 Wiley Periodicals, Inc.

Sample	Solvent casted films		Breath figure films	
	CA water / °	CA dodecane / °	CA water / °	CA dodecane / °
PS89-*b*-PFSF4	111	73	116	72
PS89-*b*-PFSF4 peeled	-	-	130	45
PS28-*b*-PFMA6	116	68	118	85
PS28-*b*-PFMA6 peeled	-	-	153	93
PS74-*b*-PFS74	96	52	112	30
PS74-*b*-PFS74 peeled	-	-	155	18
PS-*b*-PFS-COOH	93	7	106	47
PS-*b*-PFS-GlcAc4	75	<5	100	10
PS-*b*-PFS-GlcOH	70	<5	89	-

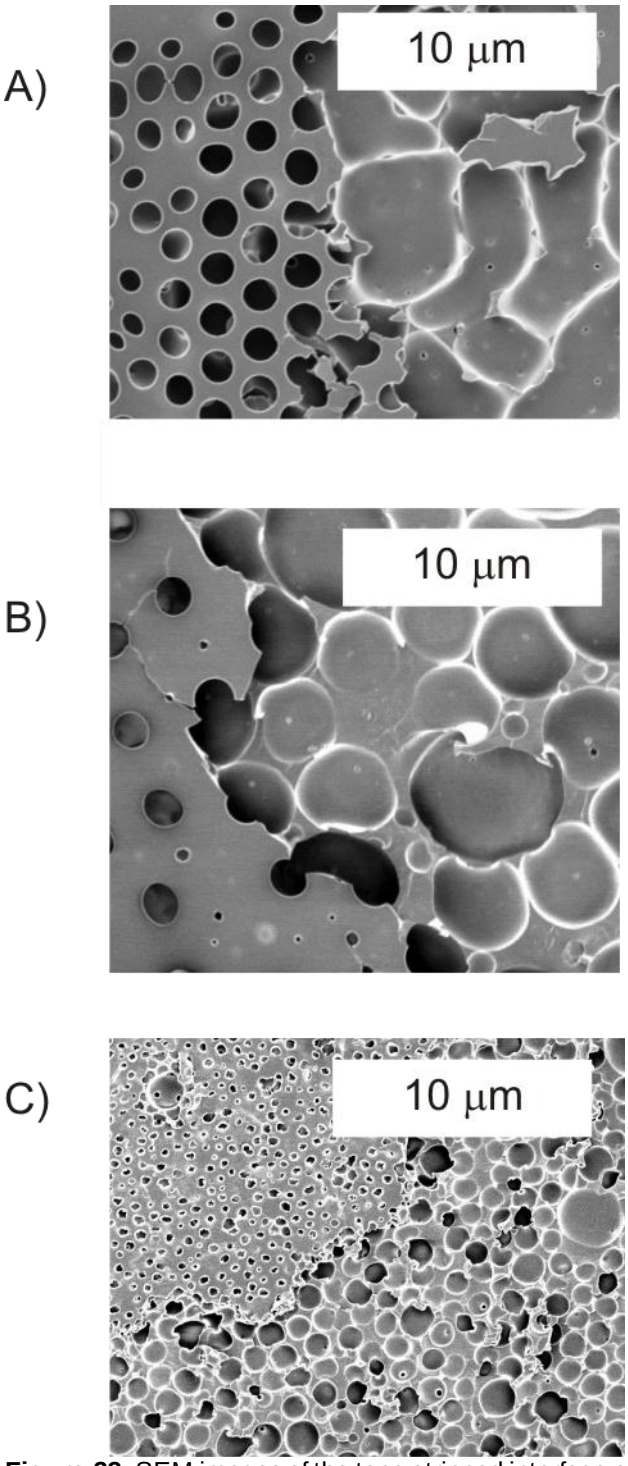

Figure 22. SEM images of the tape stripped interface of honeycomb structured films of A) PS74-*b*-PFS52 B) PS28-*b*-PFMA6 and C) PS89-*b*-PFSF4. Polymer concentrations 50 gl^{-1} in $CHCl_3$. Adapted with permission from Publication III. © 2014 Wiley Periodicals, Inc.

For glucopyranose or thioglycolic acid containing polymers the CA_{water} and $CA_{dodecane}$ are significantly lower than that of PS74-*b*-PFS74. For the deprotected glucose modified film, PS-*b*-PFS-GlcOH, the surface becomes hydrophilic (CA_{water} <90°) both for a flat solvent casted film and the BF film. Tailoring the surfaces hydrophobicity or hydrophilicity is beneficial when

thinking about possible applications like in detection of water-soluble biomarkers, because the analytes can more efficiently wet the pores beneath the surface.

4.8 AGGREGATE ANALYSIS (I, II)

Surface tension measurements showed that discussed copolymers decreased the surface tension of toluene. DLS as well as SLS measurements were used to study what kind of structures these semifluorinated copolymers formed in a selective solvent for the fluorinated units.

4.8.1 EICOSANOL METHACRYLATE BASED COPOLYMERS (I)

Aggregation of EIMA and FMA copolymers in toluene were monitored by DLS. An apparent linear increase in scattering intensity against concentration is shown in Figure 23a.

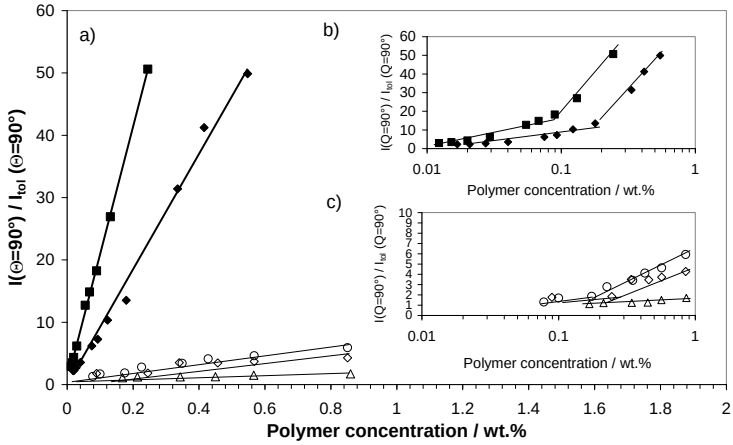

Figure 23. Normalised light scattering intensity from copolymer-toluene solutions plotted against the polymer concentration in a) PEIMA-*b*-PFMA (■),PEIMA-*b*-PFMA, heat treated at 50°C (♦), P(EIMA-FMA)-20% (Δ), P(EIMA-FMA)-50% (◊) and P(EIMA-FMA)-60% (○). Insets b) and c) show the same data plotted against the logarithm of polymer concentration. Adapted with permission from Publication I. © 2008 John Wiley & Sons, Ltd.

This behavior is different from those by Turberg and Brady[95] for semifluorinated hydrocarbons in fluorinated solvents and by Lo Nostro *et al.*[14,96] for semifluorinated n-alkane in perfluorooctane,[96] or for a semifluorinated copolymer in a fluorocarbon/hydrocarbon mixture.[14] However, when the data is plotted against the logarithm of the polymer concentration, an upward turn in the scattering intensity is observed for the solutions of highly fluorinated (>30 wt%) random copolymers at concentrations around 0.3 wt% and for the block copolymer solutions at around 0.1 wt%. This is roughly at the same concentration regime as the leveling off of the surface tension curves in Figure 6. For the random

copolymers with fluorine content >30 wt% DLS measurements revealed aggregates with R_h of the order of 5 to 10 nm with monomodal size distribution as shown in Figure 24.

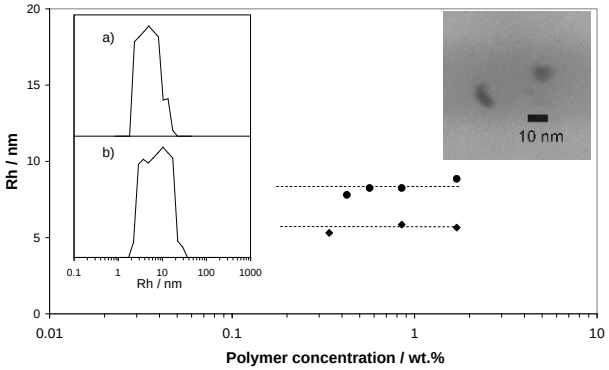

Figure 24. Hydrodynamic radii of the copolymer solutions plotted against the polymer concentration, and typical distributions of the hydrodynamic radii, P(EIMA-FMA)-50% (♦, a), P(EIMA-FMA)-60% (●, b). TEM micrograph shown is P(EIMA-FMA)-50%. Adapted with permission from Publication I. © 2008 John Wiley & Sons, Ltd.

With an increase in fluorine content of the copolymers the size of the aggregates was increased. The average R_h of the order of 5-10 nm of the aggregates is larger than what has been observed for aggregates of lower molecular weight semifluorinated substances.[14,95,96] The R_h kept constant regardless of the concentration once the aggregates were detected. This was also observed for a semifluorinated copolymer in fluorocarbon/hydrocarbon mixture by Lo Nostro *et al.*[14]

In the case of the block copolymer solutions the scattering intensity curve has an upward turn at much lower concentration than observed for random copolymers and the scattering is more intense as was shown in Figure 23. The size distributions of the block copolymer aggregates are narrow, see Figure 25.

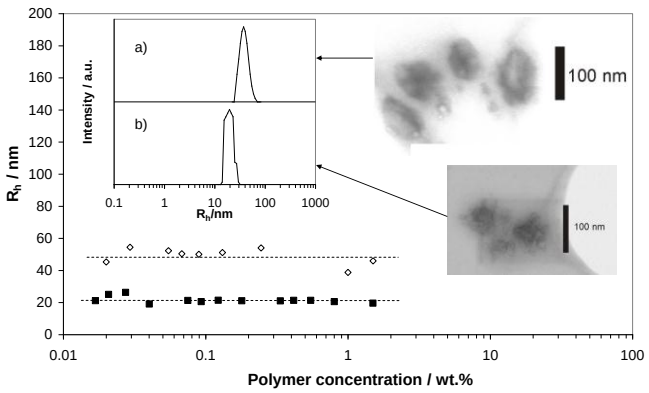

Figure 25. Hydrodynamic radii of the aggregated block copolymer solutions plotted against the polymer concentration, lines are to guide the eye only. Typical distributions of the hydrodynamic radii and corresponding TEM micrographs are plotted in the inset. PEIMA-*b*-PFMA (◊, a), PEIMA-*b*-PFMA, heat-treated at 50°C (■, b). Adapted with permission from Publication I. © 2008 John Wiley & Sons, Ltd.

Also the size of the block copolymer aggregates is much larger compared with the random copolymers, of the order of R_h ~ 50 nm for a sample dissolved at room temperature. This large difference in the sizes may originate from unequilibrium structures and thus the samples were kept overnight at elevated temperatures. Indeed, after heating at 50°C aggregates of the order of 20 nm were observed, with much lower scattering intensity. Heating at higher temperatures up to 105 °C did not lead to further reorganization of the structures.

The effect of heat treatment was also ascertained by TEM measurements. The TEM micrographs shown in Figure 25 for the sample dissolved at room temperature show non-spherical structures, of the order of 60-100 nm in length and few tens of nm in width and thus correspond well to the light scattering data. The TEM micrographs of the heat-treated sample shown in Figure 25 show spherical structures of the order 40-50 nm and thus the hydrodynamic sizes observed by DLS agree well with the TEM data.

Molecular weight of P(EIMA-FMA)-50% aggregates were estimated by Zimm analysis, see Figure 26a. Analysis gave a value of molecular weight, Mw,agg, of 421000 $gmol^{-1}$ and thus, using the molecular weight from the SEC analysis (34000 $gmol^{-1}$), aggregation number, N_{agg}, of 12 is obtained. For the random copolymer P(EIMA-FMA)-50% no angular dependence of the static light scattering intensity was observed. According to the TEM micrographs of the P(EIMA-FMA)-50% sample the aggregates of the order of 10 nm in diameter are spherical, agreeing well with the light scattering experiments. Heating the solutions overnight at 50°C did not change the particle sizes.

In the case of a block copolymer solution prepared at room temperature notable angular dependence of the scattering intensity was observed, Figure 26b. The R_g value the sample was 88 nm which leads to R_g/R_h value close to 2, indicating non-spherical geometry. The $M_{w,agg}$ $1.8*10^7$ $gmol^{-1}$ leads to an aggregation number (N_{agg}) of 2900 using the molecular weight of individual polymer (M_w=14200 $gmol^{-1}$) determined by SEC. Heating the PEIMA-*b*-PFMA solutions at 50°C overnight induced rearrangements in the aggregates. The light scattering intensity decreased and the upward turn occurred at higher polymer concentration as seen in Figure 25. The average R_h value for the heat-treated sample was 20 nm throughout the studied range of concentrations, and the samples did not show angular dependence. The Zimm plot shown in Figure 26c gave a $M_{w,agg}$ of $4.1*10^6$ $gmol^{-1}$ which means that the N_{agg} decreased to 127.

Comparison of the aggregates formed by PEIMA-*b*-PFMA to other fluorinated block copolymers in solutions shows similar features with regards to size and shape. A poly(methyl methacrylate)-*block*-poly(2-perfluorooctyl ethyl methacrylate) diblock copolymer with M_w of 78400

gmol^{-1} was reported by Imae *et al.*[97] to form spherical self-assemblies with R_h of the order ~30 nm in acetonitrile. Matsumoto *et al.*[100] studied association behavior of poly(sodium methacrylate)-*block*-poly(nonafluorohexyl methacrylate) (NaMA-*b*-NFHMA) copolymers in aqueous solutions and observed that the fluorine containing block copolymers formed micelles with bimodal size distribution. The R_h of the micelles was reported to be 26 and 140 nm for the $NaMA_{72}$-*b*-$NFHMA_{33}$ polymer and 48 and 250 nm for the $NaMA_{64}$-*b*-$NFHMA_{57}$ polymer. From the SANS data the authors concluded that the larger micelles are rodlike instead of spherical. Zhou *et al.*[99] reported that a water-soluble fluorinated triblock copolymer poly(ethylene oxide)-*b*-poly(styrene)-*b*-1,2-polybutadiene:$C_6F_{13}I$ forms an ellipsoidal structure in aqueous solutions.

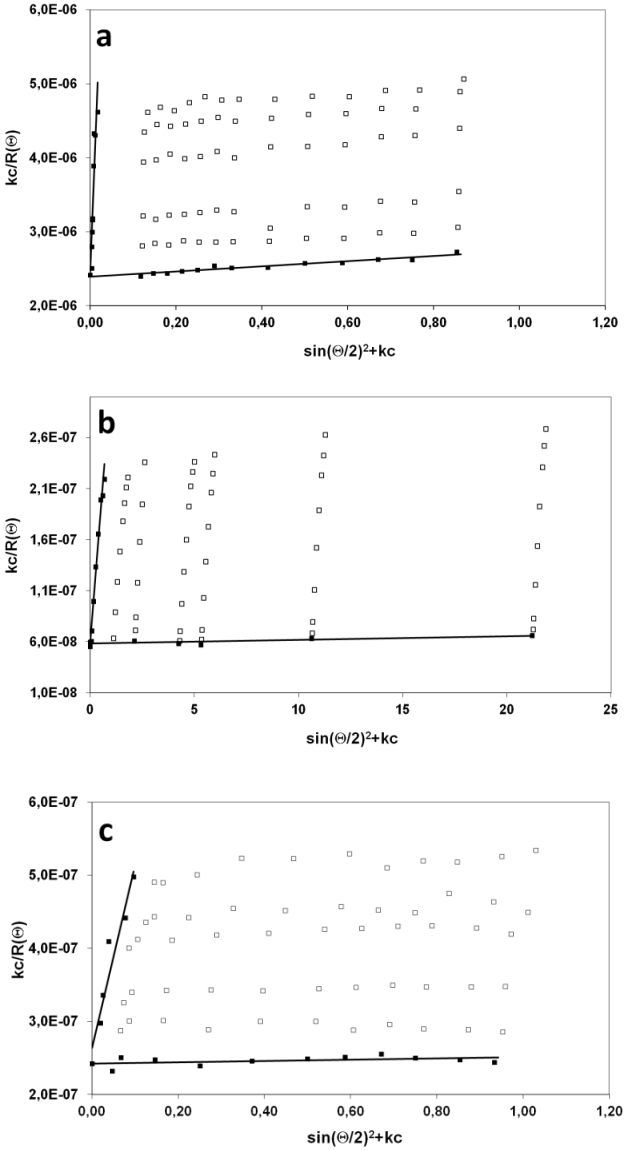

Figure 26. Zimm plots of P(EIMA-FMA)-50% solution (a), PEIMA-b-PFMA solution (b) and heat treated PEIMA-*b*-PFMA solution (c). Adapted with permission from Publication I. © 2008 John Wiley & Sons, Ltd.

4.8.2 AGGREGATE ANALYSIS OF PS BASED BLOCK COPOLYMERS (II)

DLS was used to study the aggregates formed in solution of the different polystyrene based polymers. It is known that the fluorinated blocks phase separate efficiently from the PS blocks in solution. However, no scattering were detected for PS-*b*-PFSF and PS-*b*-PEMS polymers in toluene at studied concentration range by DLS. On the other hand, solutions of polymers with other fluorinated blocks, PS-*b*-PFMA and PS-*b*-PFS, clearly aggregate and hence strongly scatter light. The different size distributions obtained are shown in Figure 27.

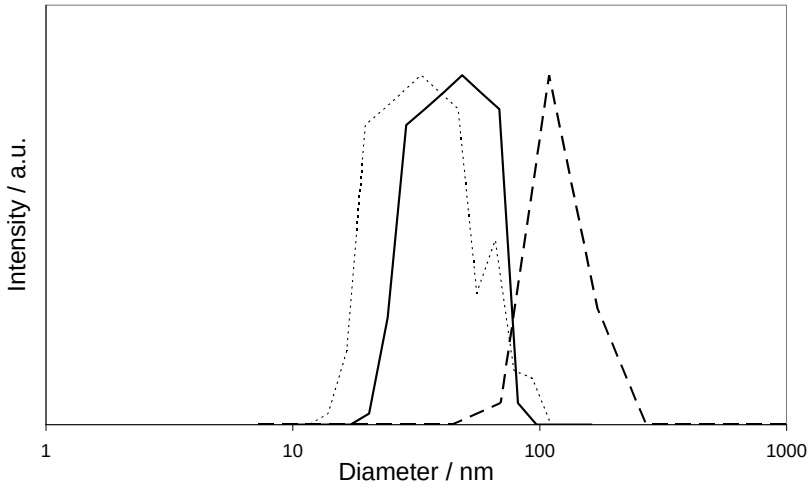

Figure 27. Size distributions of the aggregated solutions, PS89-*b*-PFMA11 (full line), PS28-*b*-PFMA6 (dashed line) and PS35-*b*-PFS35 (dotted line). Adapted with permission from Publication II. © 2009 Elsevier Ltd.

The PS89-*b*-PFMA11 polymer showed aggregates with average R_h ~20 nm. In the case of a PS28-*b*-PFMA6, the aggregates are significantly larger, with mean R_h ~60 nm. This means that the aggregation number for the larger PS28-*b*-PFMA6 polymer is higher than what it is for PS89-*b*-PFMA11. This can be explained on the basis of the properties and length of the fluorinated block. When the rigid fluorinated block is long enough, it limits the curvature of the core of the micelles and thus results in lower aggregation number. In PS-*b*-PFS polymers the fluorine containing blocks are much longer than in the other studied polymers and although the poly(pentafluorostyrene) does not have as high surface activity as the polymers with CF_3 groups, the length of the blocks induce phase separation. The length of the PFS block did not significantly influence on the size distribution of the aggregates. Thus also for these polymers the aggregation number tends to decrease slightly for the polymers having longer PFS blocks.

4.9 LECTIN BINDING AND FLUORESCENCE STUDIES (IV)

The binding of lectin to the glycosylated polymer particles was studied by DLS. Water solution of lectin Con A was titrated with nanoparticle solution to see if the multivalent glucose bearing particles are capable to interact with lectin leading to aggregation. The result can be seen from Figure 28. The interaction between lectin and nanoparticles is based on reversible multivalent sugar-protein interactions and it was also possible to break down the formed aggregates by adding glucose as competing analyte as can be seen from Figure 28. All the three types of nanoparticles showed similar behavior.

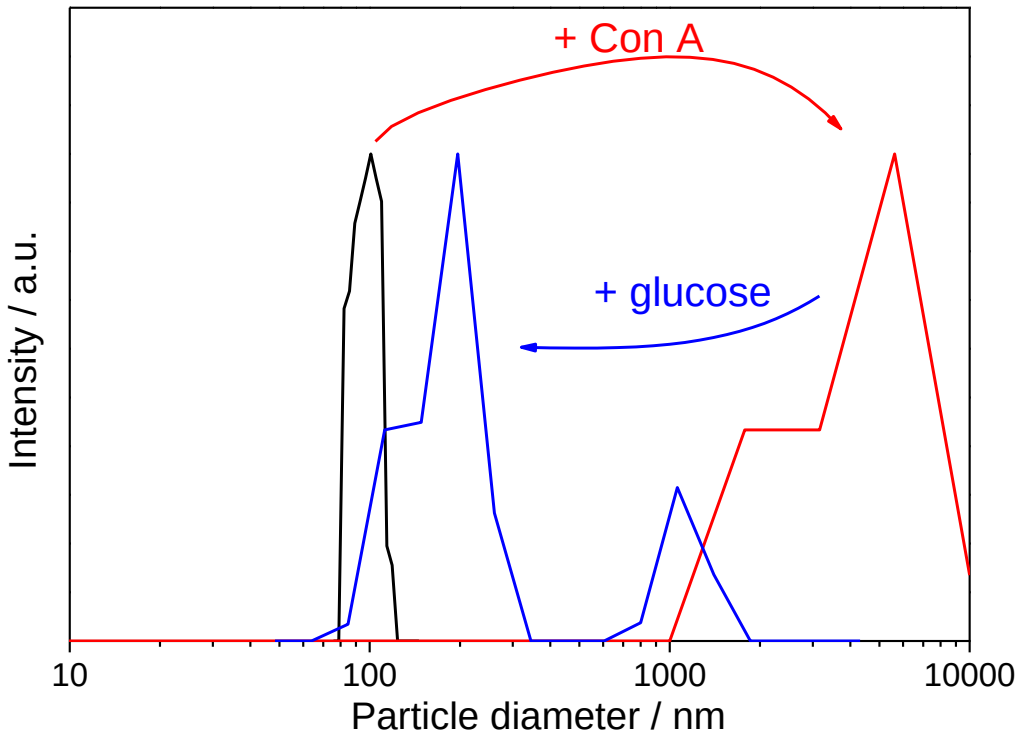

Figure 28. Change in size distributions of Glu-Mic aggregates. Original Glu-Mic (black) nanoparticle dispersion, titration with lectin Con A (red) and addition of glucose (blue).

Fluorescence Resonance Energy Transfer (FRET) technique was selected to study the interactions of the fluorescein labeled lectin (ConA-FITC) and rhodamine B isothiocyanate (RITC) labeled nanoparticles. FRET is a tool for detecting interactions and the length scales of interacting species.[146,147] In this study fluorescein labeled lectin acted as a donor and RITC labeled nanoparticles as acceptor. The fluorescent probes were selected in a fashion that the other probe, donor, absorbs at a certain excitation wavelength where the other, acceptor, does not. On the other hand, the emission of the donor probe should overlap with the absorption of the acceptor probe leading to

FRET. This means that the emission of the acceptor moieties is only possible when the two probes are sufficiently close to each other.

From Figure 29 we can see clearly that FRET occurs when RITC labeled nanoparticles is added to the solution. Signal of RITC starts to increase upon addition of the nanoparticles indicating close proximity of the probes.

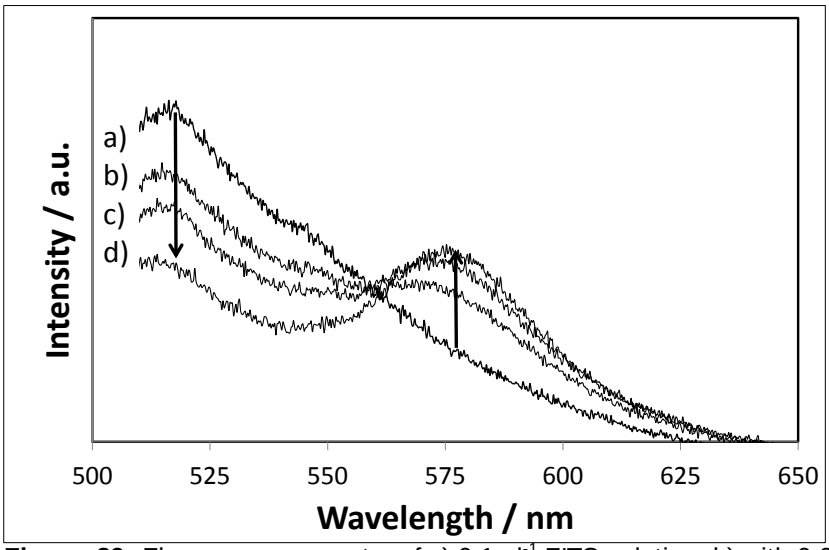

Figure 29. Fluorescence spectra of a) 0.1 gl^{-1} FITC solution, b) with 0.05 mg, c) 0.1 mg and d) 0.18 mg of RITC labeled Glu-Mic nanoparticle solution added. Adapted with permission from Publication IV. © 2014 Elsevier Ltd.

The fluorescence intensity ratio of the signals of FITC (520 nm) and RITC (580 nm) were compared to rule out any dilution effects. In Figure 30 the FRET signals are compared against mass concentration of nanoparticles added. It can be seen that Glu-Mic nanoparticles give highest FRET signal.

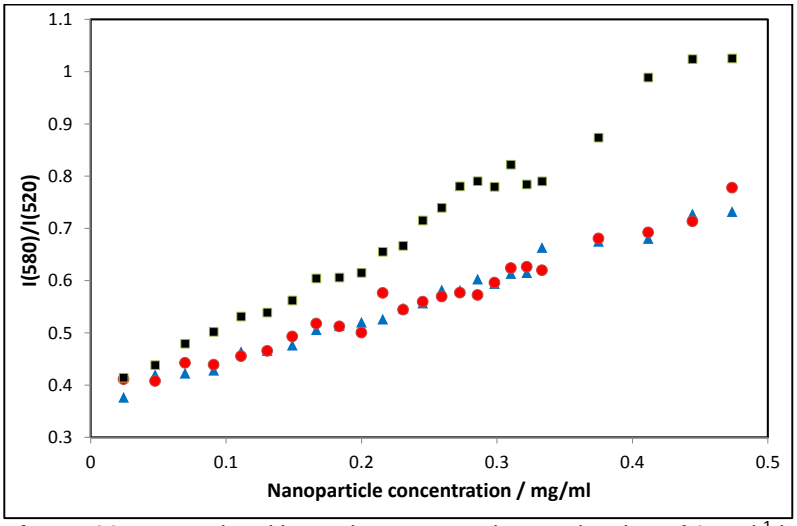

Figure 30. FRET signal intensity measured upon titration of 0.1 gl^{-1} lectin (Con A-FITC) solution with the nanoparticle (RITC) solution, (■) Glu-Mic, (▲) Glu-AP1, (●) Glu-AP2. Adapted with permission from Publication IV. © 2014 Elsevier Ltd.

However, when the measured glucose concentration of different nanoparticle solutions is taken into account the Glu-AP2 nanoparticles have the highest slope, see Figure 31. Thus the post-modification of the PS-*b*-PFS nanoparticles yields the most lectin sensitive particles, as in these the glucose moieties are solely on the surfaces.

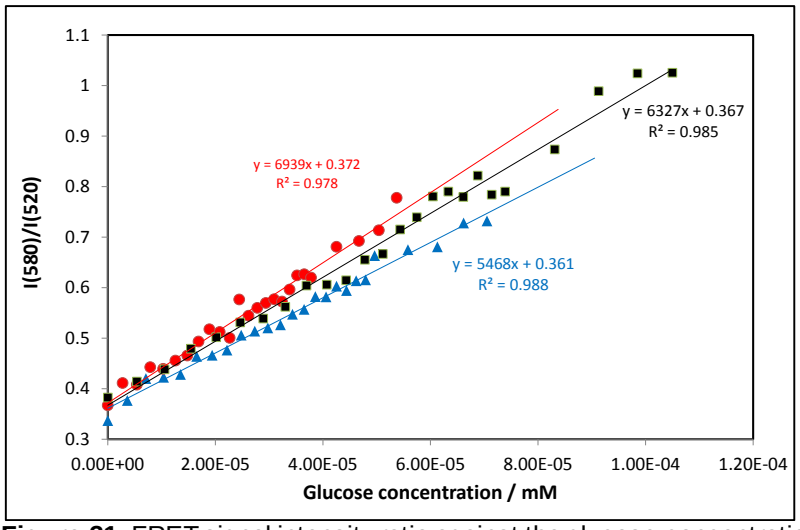

Figure 31. FRET signal intensity ratio against the glucose concentration upon titration of 0.1 gl^{-1} lectin solution with the nanoparticles, (■) Glu-Mic, (▲) Glu-AP1, (●) Glu-AP2. Adapted with permission from Publication IV. © 2014 Elsevier Ltd.

4.10 BIORECOGNITION UTILIZING BF FILMS (III)

Fluorescent ConA-FITC and RITC were also used to study the ligand binding capability of PS-*b*-PFS-GlcOH films. For control, porous PS-*b*-PFS and PS-*b*-PFS-COOH films were studied. In Figure 32 the fluorescence images taken of fluorescently labeled films at 1 µm depth from the surface are shown. The PS-*b*-PFS, PS-*b*-PFS-COOH BF films, Figure 32a, show only weak fluorescence signals regardless of the scanning depth. Similar result can be seen from Figure 32c where RITC is used as fluorescent marker. Both samples thus show that the marker is effectively removed during the washing step, apart from maybe a small amount of marker trapped in the pores. On the other hand, the BF film of PS-*b*-PFS-GlcOH, Figure 32b, shows that Con A-FITC gives intense fluorescence signal mainly from the pore walls at the selected depth focus. Deeper scanning depth showed that also the bottom of PS-*b*-PFS-GlcOH is covered with the fluorescence marker. This is also the case of fluorescence marker, RITC, which is able to bind to glucose moieties via the reaction of isothiocyanate groups, see Figure 32d. These findings indicate that the glucose bearing BF films have capability of binding the fluorescent markers both via specific protein-sugar interactions in the case of ConA and via chemical reactions in the case of rhodamine B.

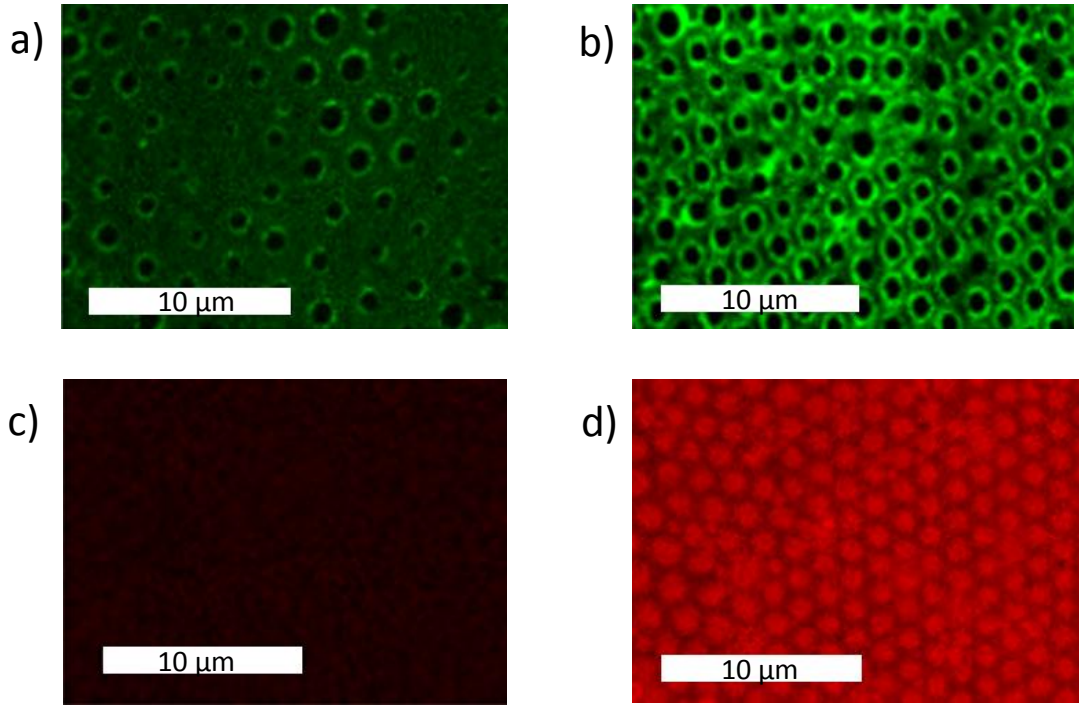

Figure 32. Cross sectional images of confocal microscopy obtained from the films stained with Con A-FITC (a PS-*b*-PFS, b PS-*b*-PFS-GlcOH) and RITC (c PS-*b*-PFS, d PS-*b*-PFS-GlcOH). Adapted with permission from Publication III. © 2014 Wiley Periodicals, Inc.

5 CONCLUSIONS

The objectives of the present research were the synthesis and characterization of organosoluble semifluorinated block copolymers. Copolymers solution properties were studied and they were used for constructing different kind of functional surfaces or nanoparticles. Polymers were prepared either by free radical solution polymerization or by atom transfer radical polymerization. Free radical solution polymerization yielded random copolymers and ATRP was used to build block copolymers.

In the case of eicosanol methacrylate based copolymers the surface properties in toluene were found to depend on the comonomer ratio and structure. With increasing fluorine content lower minimum surface tensions were found for the random copolymers. The copolymers with fluorine content >30 wt% showed aggregation behaviour in toluene solutions at low polymer concentrations. Spherical aggregates with R_h around 5-10 nm were observed by dynamic light scattering at concentrations above CMC for the random copolymers and non-spherical aggregates with diameter around 100 nm for the block copolymer. The aggregate structure of the block copolymer was shown to be temperature dependent. Heating the polymer solution resulted in the formation of smaller spherical aggregates.

Diblock copolymers based on polystyrene and various fluorinated blocks were made via ATRP and the properties of different monomers on polymer properties compared. These organosoluble polymers showed enhanced surface activity in toluene due to the fluorinated blocks. The polymers having CF_3 groups at the ends of the fluorinated alkyl side chains had notably higher surface activity compared with materials having poly(pentafluorostyrene) as the fluorinated block. Due to the incompatibility of the fluorinated blocks with polystyrene or the solvent medium, aggregation of the polymers was observed in most cases when the fluorinated block was long enough.

Selected block copolymers were then used in electrospinning. The surface properties of the fibrous or particle containing surfaces were then compared with those of solvent casted films. Superhydrophobicity, contact angle of 150° for water, were observed for electrospun polymers bearing CF_3 groups, while solvent casted films of the same polymers had contact angles typical for surface enriched fluorinated compounds, ~120°. Additionally, mixtures of these fluorinated block copolymers with polystyrene were electrospun. The surfaces were found to retain their hydrophobicity nearly on a constant level down to fluorinated block copolymer concentration of 10 wt% to that of polystyrene.

Glucose functionalised nanoparticles were made via post-polymerization functionalization of polystyrene-block-poly(pentafluorostyrene), PS-b-PFS, with para-fluorine click reaction with thio-glucopyranose. High degrees (>90%) of glucose substitution of the PFS units was achieved when the reaction took place in solution. The modified polymers were made to nanoparticles either by titration based aggregation, nanoprecipitation, from solution or by aerosol method. It was also shown that the post-functionalization of PS-b-PFS aerosol particles with the thiol para-fluorine reaction is possible and leads to glucose attachment on the surface of the particles. Furthermore, labeling of the nanoparticles with fluorescent probes is possible utilising the reaction between the glucose hydroxyls and an isothiocyanate marker.

Interactions of the glycosylated nanoparticles with a fluorescent lectin were studied. It was shown that the nanoparticles bind lectins which leads to their aggregation. Fluorescence resonance energy transfer (FRET) studies on rhodamine labelled nanoparticles also revealed differences in the binding of lectin between different types of the nanoparticles.

Honeycomb structured films utilising breath figure (BF) templating technique were made from selected block copolymers. Porous films with pore sizes from 0.2 μm to 1.7 μm depending on the polymer used and the polymer concentration were obtained. The surfaces of the porous films containing only hydrophobic blocks were more hydro- and oleophobic than flat solvent casted films due to the increased roughness. Peeling off the top layer further increased the roughness and the hydrophobicity increased, leading to superhydrophobic surfaces in case of PS-*b*-PFS and PS-*b*-PFMA. The pentafluorostyrene units of the PS-*b*-PFS were further modified with thioglycolic acid or a thiolated glucopyranose. Water contact angles decreased with the introduction of hydrophilic units and for the glucose modified BF film, PS-*b*-PFS-GlcOH, the surface turned hydrophilic with water contact angle <90°. Finally, fluorescence microscopy showed that the pores of the glucose containing BF films bind fluorescent markers lectin Con A-FITC via specific protein-sugar interactions and rhodamine B isothiocyanate by a chemical reaction between the glucose units and isothiocyanate.

6 REFERENCES

(1) Simons, J. H.; Block, L. P. *J. Am. Chem. Soc.* **1937**, *59*, 1407–1407.
(2) Imae, T. *Curr. Opin. Colloid Interface Sci.* **2003**, *8*, 307–314.
(3) Hirao, A.; Sugiyama, K.; Yokoyama, H. *Prog. Polym. Sci.* **2007**, *32*, 1393–1438.
(4) Hansen, N. M. L.; Jankova, K.; Hvilsted, S. *Eur. Polym. J.* **2007**, *43*, 255–293.
(5) Kissa, E. *Fluorinated Surfactants*; Surfactant Science Series; Dekker, 1994; Vol. 50.
(6) Borkar, S.; Jankova, K.; Siesler, H. W.; Hvilsted, S. *Macromolecules* **2004**, *37*, 788–794.
(7) Nenov, S.; Clark, C. G.; Klapper, M.; Müllen, K. *Macromol. Chem. Phys.* **2007**, *208*, 1362–1369.
(8) Lacroix-Desmazes, P.; Andre, P.; Desimone, J. M.; Ruzette, A.-V.; Boutevin, B. *J. Polym. Sci. Part Polym. Chem.* **2004**, *42*, 3537–3552.
(9) Li, X.; Andruzzi, L.; Chiellini, E.; Galli, G.; Ober, C. K.; Hexemer, A.; Kramer, E. J.; Fischer, D. A. *Macromolecules* **2002**, *35*, 8078–8087.
(10) Fulton, J. L.; Pfund, D. M.; McClain, J. B.; Romack, T. J.; Maury, E. E.; Combes, J. R.; Samulski, E. T.; DeSimone, J. M.; Capel, M. *Langmuir* **1995**, *11*, 4241–4249.
(11) Morita, M.; Kubo, M.; Matsumoto, M. *Colloids Surf. Physicochem. Eng. Asp.* **1996**, *109*, 183–194.
(12) Morita, M.; Matsumoto, M.; Usui, S.; Abe, T.; Denkov, N.; Velev, O.; Ivanov, I. B. *Colloids Surf.* **1992**, *67*, 81–93.
(13) Antonietti, M.; Förster, S.; Micha, M. A.; Oestreich, S. *Acta Polym.* **1997**, *48*, 262–268.
(14) Nostro, P. L.; Ku, C. Y.; Chen, S.-H.; Lin, J.-S. *J. Phys. Chem.* **1995**, *99*, 10858–10864.
(15) Huang, W.; Jin, C.; Derzon, D. K.; Huber, T. A.; Last, J. A.; Provencio, P. P.; Gopalan, A. S.; Dugger, M.; Sasaki, D. Y. *J. Colloid Interface Sci.* **2004**, *272*, 457–464.
(16) Twieg, R. J.; Russell, T. P.; Siemens, R.; Rabolt, J. F. *Macromolecules* **1985**, *18*, 1361–1362.
(17) Ku, C.-Y.; Lo Nostro, P.; Chen, S.-H. *J. Phys. Chem. B* **1997**, *101*, 908–914.
(18) Abdallah, D. J.; Weiss, R. G. *Adv. Mater.* **2000**, *12*, 1237–1247.
(19) Krupers, M. J.; Bartelink, C. F.; Grünhauer, H. J. M.; Moller, M. *Polymer* **1998**, *39*, 2049–2053.
(20) Hu, S., W.; Griffith, J., R. *Polym Prepr **1993***, 23, 401–402.
(21) Kim, E.; Cho, S. Y.; Yeu, D.-M.; Shin, S.-Y. *Chem. Mater.* **2005**, *17*, 962–966.
(22) Yoshimura, R.; Hikita, M.; Tomaru, S.; Imamura, S. *J. Light. Technol.* **1998**, *16*, 1030–1037.
(23) DeRosa, T. F.; Kaufman, B. J.; Sung, R. L. M.; Russo, J. M. *Polymer Prepr.* **1994**, 34, 718–720.
(24) Saïdi, S.; Guittard, F.; Guimon, C.; Géribaldi, S. *J. Polym. Sci. Part Polym. Chem.* **2005**, *43*, 3737–3747.
(25) Volkov, V. V.; Fadeev, A. G.; Plate, N. A.; Amaya, N.; Murata, Y.; Takanara, A.; Kajiyama, T. *Polym. Bull.* **1994**, *32*, 193–200.
(26) Becer, C. R.; Babiuch, K.; Pilz, D.; Hornig, S.; Heinze, T.; Gottschaldt, M.; Schubert, U. S. *Macromolecules* **2009**, *42*, 2387–2394.

(27) De León, A. S.; del Campo, A.; Fernández-García, M.; Rodríguez-Hernández, J.; Muñoz-Bonilla, A. *ACS Appl. Mater. Interfaces* **2013**, *5*, 3943–3951.
(28) Becer, C. R.; Hoogenboom, R.; Schubert, U. S. *Angew. Chem. Int. Ed.* **2009**, *48*, 4900–4908.
(29) Babiuch, K.; Wyrwa, R.; Wagner, K.; Seemann, T.; Hoeppener, S.; Becer, C. R.; Linke, R.; Gottschaldt, M.; Weisser, J.; Schnabelrauch, M.; Schubert, U. S. *Biomacromolecules* **2011**, *12*, 681–691.
(30) León, A. S. de; Campo, A. del; Labrugère, C.; Fernández-García, M.; Muñoz-Bonilla, A.; Rodríguez-Hernández, J. *Polym. Chem.* **2013**, *4*, 4024–4032.
(31) Nishimura, S.; Nagai, A.; Takahashi, A.; Narita, T.; Hagiwara, T.; Hamana, H. *Polym. J.* **1990**, *22*, 171–174.
(32) Kurosawa, S.; Hirokawa, T.; Kashima, K.; Aizawa, H.; Han, D.-S.; Yoshimi, Y.; Okada, Y.; Yase, K.; Miyake, J.; Yoshimoto, M.; Hilborn, J. *Thin Solid Films* **2000**, *374*, 262–267.
(33) Han, L. M.; Timmons, R. B.; Lee, W. W.; Chen, Y.; Hu, Z. *J. Appl. Phys.* **1998**, *84*, 439–444.
(34) Pryor, W. A.; Huang, T.-L. *Macromolecules* **1969**, *2*, 70–77.
(35) Bartlett, B.; Buckley, L. J.; Godbey, D. J.; Schroeder, M. J.; Fontenot, C.; Eisinger, S. *J. Vac. Sci. Technol. B* **1999**, *17*, 90–94.
(36) Pitois, C.; Vukmirovic, S.; Hult, A.; Wiesmann, D.; Robertsson, M. *Macromolecules* **1999**, *32*, 2903–2909.
(37) Jankova, K.; Hvilsted, S. *Macromolecules* **2003**, *36*, 1753–1758.
(38) Gudipati, C. S.; Tan, M. B. H.; Hussain, H.; Liu, Y.; He, C.; Davis, T. P. *Macromol. Rapid Commun.* **2008**, *29*, 1902–1907.
(39) Becer, C. R. *Macromol. Rapid Commun.* **2012**, *33*, 742–752.
(40) Lazzari, M.; Aglietto, M.; Castelvetro, V.; Chiantore, O. *Chem. Mater.* **2001**, *13*, 2843–2849.
(41) Morita, M.; Ogisu, H.; Kubo, M. *J. Appl. Polym. Sci.* **1999**, *73*, 1741–1749.
(42) Krupers, M. J.; Möller, M. *J. Fluor. Chem.* **1997**, *82*, 119–124.
(43) Guyot, B.; Ameduri, B.; Boutevin, B.; Melas, M.; Viguier, M.; Collet, A. *Macromol. Chem. Phys.* **1998**, *199*, 1879–1885.
(44) Mayes, A. G.; Mosbach, K. *Anal. Chem.* **1996**, *68*, 3769–3774.
(45) Krupers, M. J.; Sheiko, S. S.; Möller, M. *Polym. Bull.* **1998**, *40*, 211–217.
(46) Betts, D. E.; Johnson, T.; LeRoux, D.; DeSimone, J. M. *1998*, 418–432.
(47) Xia, J.; Johnson, T.; Gaynor, S. G.; Matyjaszewski, K.; DeSimone, J. *Macromolecules* **1999**, *32*, 4802–4805.
(48) Li, K.; Wu, P.; Han, Z. *Polymer* **2002**, *43*, 4079–4086.
(49) Perrier, S.; Jackson, S. G.; Haddleton, D. M.; Ameduri, B.; Boutevin, B. *Tetrahedron* **2002**, *58*, 4053–4059.
(50) Perrier, S.; Jackson, S. G.; Haddleton, D. M.; Améduri, B.; Boutevin, B. *Macromolecules* **2003**, *36*, 9042–9049.
(51) Yang, Y.; Wang, Z.; Gao, Y.; Liu, T.; Hu, C.; Dong, Q. *J. Appl. Polym. Sci.* **2006**, *102*, 1146–1151.
(52) Shemper, B. S.; Mathias, L. J. *Eur. Polym. J.* **2004**, *40*, 651–665.
(53) Lim, K. T.; Lee, M. Y.; Moon, M. J.; Lee, G. D.; Hong, S.-S.; Dickson, J. L.; Johnston, K. P. *Polymer* **2002**, *43*, 7043–7049.
(54) Hussain, H.; Busse, K.; Kressler, J. *Macromol. Chem. Phys.* **2003**, *204*, 936–946.
(55) Hussain, H.; Budde, H.; Höring, S.; Busse, K.; Kressler, J. *Macromol. Chem. Phys.* **2002**, *203*, 2103–2112.
(56) Zhang, Z.-B.; Ying, S.-K.; Shi, Z.-Q. *Polymer* **1999**, *40*, 5439–5444.
(57) Zhang, Z. B.; Ying, S. K.; Hu, Q. H.; Xu, X. D. *J. Appl. Polym. Sci.* **2002**, *83*, 2625–2633.

(58) Radhakrishnan, K.; Switek, K. A.; Hillmyer, M. A. *J. Polym. Sci. Part Polym. Chem.* **2004**, *42*, 853–861.
(59) Jankova, K.; Hvilsted, S. *J. Fluor. Chem.* **2005**, *126*, 241–250.
(60) Fu, G. D.; Kang, E. T.; Neoh, K. G. *Langmuir* **2005**, *21*, 3619–3624.
(61) Ma, Z.; Lacroix-Desmazes, P. *J. Polym. Sci. Part Polym. Chem.* **2004**, *42*, 2405–2415.
(62) Eberhardt, M.; Théato, P. *Macromol. Rapid Commun.* **2005**, *26*, 1488–1493.
(63) Inoue, Y.; Watanabe, J.; Takai, M.; Yusa, S.; Ishihara, K. *J. Polym. Sci. Part Polym. Chem.* **2005**, *43*, 6073–6083.
(64) Roche, V.; Vacandio, F.; Bertin, D.; Massiani, Y. *J. Electroceramics* **2006**, *16*, 41–47.
(65) Andruzzi, L.; Chiellini, E.; Galli, G.; Li, X.; Kang, S. H.; Ober, C. K. *J. Mater. Chem.* **2002**, *12*, 1684–1692.
(66) Choi, W. O.; Sawamoto, M.; Higashimura, T. *Polym. J.* **1988**, *20*, 201–206.
(67) Percec, V.; Lee, M. *J. Macromol. Sci. Part A* **1992**, *29*, 723–740.
(68) Höpken, J.; Möller, M.; Lee, M.; Percec, V. *Makromol. Chem.* **1992**, *193*, 275–284.
(69) Vandooren, C.; Jérôme, R.; Teysslé, P. *Polym. Bull.* **1994**, *32*, 387–393.
(70) Matsumoto, K.; Kubota, M.; Matsuoka, H.; Yamaoka, H. *Macromolecules* **1999**, *32*, 7122–7127.
(71) Castelvetro, V.; Bontà Pittaluga, G.; Ciardelli, F. *Macromol. Chem. Phys.* **2001**, *202*, 2093–2103.
(72) Shimomoto, H.; Fukami, D.; Kanaoka, S.; Aoshima, S. *J. Polym. Sci. Part Polym. Chem.* **2011**, *49*, 1174–1182.
(73) Yong, T.-M.; Hems, W. P.; Nunen, J. L. M. van; Holmes, A. B.; Steinke, J. H. G.; Taylor, P. L.; Segal, J. A.; Griffin, D. A. *Chem. Commun.* **1997**, 1811–1812.
(74) Ishizone, T.; Sugiyama, K.; Sakano, Y.; Mori, H.; Hirao, A.; Nakahama, S. *Polym. J.* **1999**, *31*, 983–988.
(75) Yang, S.; Wang, J.; Ogino, K.; Valiyaveettil, S.; Ober, C. K. *Chem. Mater.* **2000**, *12*, 33–40.
(76) Hvilsted, S.; Borkar, S.; Siesler, H. W.; Jankova, K. In *Advances in Controlled/Living Radical Polymerization*; ACS Symposium Series; American Chemical Society, 2003; Vol. 854, pp. 236–249.
(77) Qiu, J.; Matyjaszewski, K. *Macromolecules* **1997**, *30*, 5643–5648.
(78) Dimitrov, I.; Jankova, K.; Hvilsted, S. *J. Fluor. Chem.* **2013**, *149*, 30–35.
(79) Riedel, M.; Stadermann, J.; Komber, H.; Simon, F.; Voit, B. *Eur. Polym. J.* **2011**, *47*, 675–684.
(80) Hwang, H. S.; Kim, H. J.; Jeong, Y. T.; Gal, Y.-S.; Lim, K. T. *Macromolecules* **2004**, *37*, 9821–9825.
(81) Saïdi, S.; Guittard, F.; Géribaldi, S. *Polym. Int.* **2002**, *51*, 1058–1062.
(82) Krupers, M.; Möller, M. *Macromol. Chem. Phys.* **1997**, *198*, 2163–2179.
(83) Van De Grampel, R. D.; Van Geldrop, J.; Laven, J.; Van Der Linde, R. *J. Appl. Polym. Sci.* **2001**, *79*, 159–165.
(84) Ito, H.; Okazaki, M.; Miller, D. C. *J. Polym. Sci. Part Polym. Chem.* **2004**, *42*, 1506–1527.
(85) Corpart, J.-M.; Girault, S.; Juhué, D. *Langmuir* **2001**, *17*, 7237–7244.
(86) Makrikosta, G.; Georgas, D.; Siakali-Kioulafa, E.; Pitsikalis, M. *Eur. Polym. J.* **2005**, *41*, 47–54.
(87) Kumar, S. V.; Musturappa, T. E.; Prasannakumar, S.; Mahadevan, K. M.; Sherigara, B. S. *J. Macromol. Sci. Part A* **2007**, *44*, 1161–1169.
(88) Akyüz, A.; Paril, A.; Giz, A. *J. Appl. Polym. Sci.* **2006**, *100*, 3822–3827.
(89) Azzahari, A. D.; Yahya, R.; Hassan, A.; Sheikh, M. R. K. *Fibers Polym.* **2012**, *13*, 555–563.
(90) Fineman, M.; Ross, S. D. *J. Polym. Sci.* **1950**, *5*, 259–262.

(91) Tüdos, F.; Kelen, T.; Földes-berezsnich, T.; Turcsányi, B. *J. Macromol. Sci. Part - Chem.* **1976**, *10*, 1513–1540.
(92) Kato, M.; Kamigaito, M.; Sawamoto, M.; Higashimura, T. *Macromolecules* **1995**, *28*, 1721–1723.
(93) Wang, J.-S.; Matyjaszewski, K. *J. Am. Chem. Soc.* **1995**, *117*, 5614–5615.
(94) Abe, M.; Morikawa, K.; Ogino, K.; Sawada, H.; Matsumoto, T.; Nakayama, M. *Langmuir* **1992**, *8*, 763–764.
(95) Turberg, M. P.; Brady, J. E. *J. Am. Chem. Soc.* **1988**, *110*, 7797–7801.
(96) Lo Nostro, P.; Chen, S. H. *J. Phys. Chem.* **1993**, *97*, 6535–6540.
(97) Imae, T.; Tabuchi, H.; Funayama, K.; Sato, A.; Nakamura, T.; Amaya, N. *Colloids Surf. Physicochem. Eng. Asp.* **2000**, *167*, 73–81.
(98) Zhou, S.; Chu, B. *Macromolecules* **1998**, *31*, 5300–5308.
(99) Zhou, Z.; Li, Z.; Ren, Y.; Hillmyer, M. A.; Lodge, T. P. *J. Am. Chem. Soc.* **2003**, *125*, 10182–10183.
(100) Matsumoto, K.; Ishizuka, T.; Harada, T.; Matsuoka, H. *Langmuir* **2004**, *20*, 7270–7282.
(101) Busse, K.; Kressler, J.; van Eck, D.; Höring, S. *Macromolecules* **2002**, *35*, 178–184.
(102) Nakagawa, J.; Kamogawa, K.; Momozawa, N.; Sakai, H.; Kawase, T.; Sawada, H.; Sano, Y.; Abe, M. *Langmuir* **1998**, *14*, 2061–2067.
(103) Valtola, L.; Hietala, S.; Tenhu, H.; Denifl, P.; Wilen, C.-E. *Polym. Adv. Technol.* **2009**, *20*, 225–234.
(104) Valtola, L.; Koponen, A.; Karesoja, M.; Hietala, S.; Laukkanen, A.; Tenhu, H.; Denifl, P. *Polymer* **2009**, *50*, 3103–3110.
(105) Ma, M.; Mao, Y.; Gupta, M.; Gleason, K. K.; Rutledge, G. C. *Macromolecules* **2005**, *38*, 9742–9748.
(106) Agarwal, S.; Horst, S.; Bognitzki, M. *Macromol. Mater. Eng.* **2006**, *291*, 592–601.
(107) Wu, W.; Zhu, Q.; Qing, F.; Han, C. C. *Langmuir* **2009**, *25*, 17–20.
(108) Gao, J.; Yan, D.; Ni, H.; Wang, L.; Yang, Y.; Wang, X. *J. Colloid Interface Sci.* **2013**, *393*, 361–368.
(109) Hopken, J.; Moller, M. *Macromolecules* **1992**, *25*, 1461–1467.
(110) Ball, P. *Nature* **1999**, *400*, 507–509.
(111) Nakajima, A.; Hashimoto, K.; Watanabe, T. *Monatshefte Für Chem. Chem. Mon.* **2001**, *132*, 31–41.
(112) Gu, Z.-Z.; Uetsuka, H.; Takahashi, K.; Nakajima, R.; Onishi, H.; Fujishima, A.; Sato, O. *Angew. Chem. Int. Ed.* **2003**, *42*, 894–897.
(113) Barthlott, W.; Neinhuis, C. *Planta* **1997**, *202*, 1–8.
(114) Hozumi, A.; Takai, O. *Thin Solid Films* **1997**, *303*, 222–225.
(115) Guo, Y.; Tang, D.; Gong, Z. *J. Phys. Chem. C* **2012**, *116*, 26284–26294.
(116) Li, D.; Xia, Y. *Adv. Mater.* **2004**, *16*, 1151–1170.
(117) Roach, P.; Shirtcliffe, N. J.; Newton, M. I. *Soft Matter* **2008**, *4*, 224–240.
(118) Grignard, B.; Vaillant, A.; de Coninck, J.; Piens, M.; Jonas, A. M.; Detrembleur, C.; Jerome, C. *Langmuir* **2011**, *27*, 335–342.
(119) Bunz, U. H. F. *Adv. Mater.* **2006**, *18*, 973–989.
(120) Hernández-Guerrero, M.; Stenzel, M. H. *Polym. Chem.* **2012**, *3*, 563–577.
(121) Escalé, P.; Rubatat, L.; Billon, L.; Save, M. *Eur. Polym. J.* **2012**, *48*, 1001–1025.
(122) Widawski, G.; Rawiso, M.; François, B. *Nature* **1994**, *369*, 387–389.
(123) François, B.; Pitois, O.; François, J. *Adv. Mater.* **1995**, *7*, 1041–1044.
(124) Ferrari, E.; Fabbri, P.; Pilati, F. *Langmuir* **2011**, *27*, 1874–1881.
(125) Cui, L.; Peng, J.; Ding, Y.; Li, X.; Han, Y. *Polymer* **2005**, *46*, 5334–5340.
(126) Peng, J.; Han, Y.; Yang, Y.; Li, B. *Polymer* **2004**, *45*, 447–452.
(127) Stenzel, M. H.; Barner-Kowollik, C.; Davis, T. P. *J. Polym. Sci. Part Polym. Chem.* **2006**, *44*, 2363–2375.
(128) Min, E.; Wong, K. H.; Stenzel, M. H. *Adv. Mater.* **2008**, *20*, 3550–3556.

(129) Escalé, P.; Rubatat, L.; Derail, C.; Save, M.; Billon, L. *Macromol. Rapid Commun.* **2011**, *32*, 1072–1076.
(130) Hao, X.; Stenzel, M. H.; Barner-Kowollik, C.; Davis, T. P.; Evans, E. *Polymer* **2004**, *45*, 7401–7415.
(131) Saunders, A. E.; Dickson, J. L.; Shah, P. S.; Lee, M. Y.; Lim, K. T.; Johnston, K. P.; Korgel, B. A. *Phys. Rev. E* **2006**, *73*, 031608.
(132) De León, A. S.; Muñoz-Bonilla, A.; Fernández-García, M.; Rodríguez-Hernández, J. *J. Polym. Sci. Part Polym. Chem.* **2012**, *50*, 851–859.
(133) De León, A. S.; del Campo, A.; Fernández-García, M.; Rodríguez-Hernández, J.; Muñoz-Bonilla, A. *Langmuir* **2012**, *28*, 9778–9787.
(134) Hernández-Guerrero, M.; Min, E.; Barner-Kowollik, C.; Müller, A. H. E.; Stenzel, M. H. *J. Mater. Chem.* **2008**, *18*, 4718.
(135) Beattie, D.; Wong, K. H.; Williams, C.; Poole-Warren, L. A.; Davis, T. P.; Barner-Kowollik, C.; Stenzel, M. H. *Biomacromolecules* **2006**, *7*, 1072–1082.
(136) Wu, X.; Wang, S. *ACS Appl. Mater. Interfaces* **2012**, *4*, 4966–4975.
(137) Muñoz-Bonilla, A.; Ibarboure, E.; Papon, E.; Rodriguez-Hernandez, J. *Langmuir* **2009**, *25*, 6493–6499.
(138) Muñoz-Bonilla, A.; Ibarboure, E.; Papon, E.; Rodriguez-Hernandez, J. *J. Polym. Sci. Part Polym. Chem.* **2009**, *47*, 2262–2271.
(139) Yabu, H.; Takebayashi, M.; Tanaka, M.; Shimomura, M. *Langmuir* **2005**, *21*, 3235–3237.
(140) Kim, J.; Lew, B.; Kim, W. S. *Nanoscale Res. Lett.* **2011**, *6*, 616.
(141) Eerikäinen, H.; Kauppinen, E. I. *Int. J. Pharm.* **2003**, *263*, 69–83.
(142) Raula, J.; Eerikäinen, H.; Kauppinen, E. I. *Int. J. Pharm.* **2004**, *284*, 13–21.
(143) Dreywood, R. *Ind. Eng. Chem. Anal. Ed.* **1946**, *18*, 499–499.
(144) Wong, K. H.; Davis, T. P.; Barner-Kowollik, C.; Stenzel, M. H. *Polymer* **2007**, *48*, 4950–4965.
(145) Hiwatari, K.; Serizawa, T.; Seto, F.; Kishida, A.; Muraoka, Y.; Akashi, M. *33*, 669–675.
(146) Meadows, D.; Schultz, J. S. *Talanta* **1988**, *35*, 145–150.
(147) Cardullo, R. A.; Chick, W. L.; Wolf, D. E. Method and device for detecting and quantifying glucose in body fluids. US5342789 A, August 30, 1994.